Energy localization in substitutionally disordered solids. II. Studies by optical and optically detected magnetic resonance spectroscopy

D. D. Smith,[a] D. P. Millar,[b] and A. H. Zewail[c]

Arthur Amos Noyes Laboratory of Chemical Physics, [d] *California Institute of Technology, Pasadena, California 91125*

(Received 12 December 1978; accepted 25 September 1979)

In continuation of previous work, we present experimental measurements on the localization of triplet Frenkel excitons in isotopically doped phenazine and 1,4-dibromonaphthalene (2-D and 1-D *effective* excitation transfer topology, respectively). Dependence of steady state impurity aggregate (monomer, dimers, etc.) emission intensities on temperature, concentration of dopant, and the dimensionality is experimentally measured and theoretically modeled. Effects of phonons and excited state lifetimes are explicitly included in a numerical simulation of the data by average-lattice rate equations. The rate equations explain the major features of the experimental data quite well. For use in the rate equations, we have performed Monte Carlo experiments to determine cluster probabilities on 1-D and anisotropic 2-D lattices. Finally, the relevance of these findings to *Anderson localization* and *percolation theory* is discussed.

I. INTRODUCTION

In the past few decades, interest in molecular solids has largely been confined to identifying the energetic structure of Frenkel exciton (singlet and triplet state) bands.[1] More recently, dynamics of exciton transport in pure crystals (i.e., there is no impurity introduced but intrinsic impurities and defects are present) were studied to elucidate the effect of strong and weak exciton–phonon couplings on the mode of transport—coherent or incoherent.[2] Disorder of the crystals alters the energetic structure as well as the dynamics. The former has been treated by several groups for isotopically mixed crystals in the heavy-doping limit and the latter has just begun to be of interest to theorists and experimentalists.

In recent work, Kopelman *et al.*,[3] Colson *et al.*,[4] and Smith *et al.*[5] have shown experimentally that disordered naphthalene, benzene and phenazine exhibit a "critical" dopant concentration for energy transfer amongst the impurities. Kopelman *et al.*'s system consisted of naphthalene-d_8, (host), naphthalene-h_8 (trap), and beta-methylnaphthalene which acted as a low-energy trap (called a supertrap, *s*, in their publication). Exciting with a filtered xenon lamp at about 1.8 K, they observed an abrupt change in the phosphorescence intensity ratio $I_s/(I_s+I_a)$, as a function of the trap concentration, I_a being the naphthalene-h_8 energy acceptor. These studies have led Kopelman and his co-workers to conclude that percolation theory can be used to explain the results. They have made use of dynamic, static, and site percolation concepts and have used percolation to obtain exciton *coherence* lengths.

Colson and his group[4] have studied benzene isotopic mixed crystals both in the singlet and triplet states. Their low-energy trap was a chemically distinct specie, pyrazine. Energy transfer thresholds were found at 2.8% for the triplet state and about 40% for the singlet state. The thresholds were discussed in terms of percolation, pointing out that the exciton lifetime is a key factor in determining the difference in trap concentration for singlet and triplet percolation thresholds. The shorter singlet lifetime limits the energy transfer range despite the longer range coupling compared to the short range exchange coupling in the triplet state.

Smith *et al.*,[5] using isotopically doped phenazine have taken a different approach. The two component system of phenazine-h_8 in phenazine-d_8 at any concentration has h_8 monomers and dimers isolated by d_8 host. For concentrations less than 5%, the number of trimers is negligible and the dimer alone serves as a trap for monomer excitation. The ratio of dimer to monomer phosphorescence intensity as a function of h_8 concentration showed a threshold at ~5% *only* at low temperatures (1.13–1.4 K). This was interpreted as a transport threshold in the context of the Klafter–Jortner model[6] which applies the well-known theory of P. W. Anderson[7] to energy transfer in organic crystals. We did not test the applicability of classical percolation theory in our original paper (henceforth referred to as I) because of our belief, as that of Klafter and Jortner, that quantum mechanical tunneling prevails in these systems. As pointed out by Mott,[8] percolation may not be profitably applied to electron transport in microscopically homogeneous crystals.

In this paper we present quantitative steady-state studies on phenazine and 1,4-dibromonaphthalene (DBN). The effects of concentration, temperature, and dimensionality are theoretically modeled and experimentally tested. We perform a numerical simulation of experimental data using average rate equations and from the expressions derived herein present physical interpretations of the data. We discuss the relevance of the results to the Anderson and percolation models. This paper addresses itself to the very specific problem of en-

[a] This work was done in partial fulfillment of the Ph. D. requirement of D. D. Smith at the California Institute of Technology.
[b] Fulbright–Hays Graduate Student.
[c] Alfred P. Sloan Fellow, and Camille and Henry Dreyfus Teacher-Scholar.
[d] Contribution No. 5931.

 0021-9606/80/021187-22$01.00

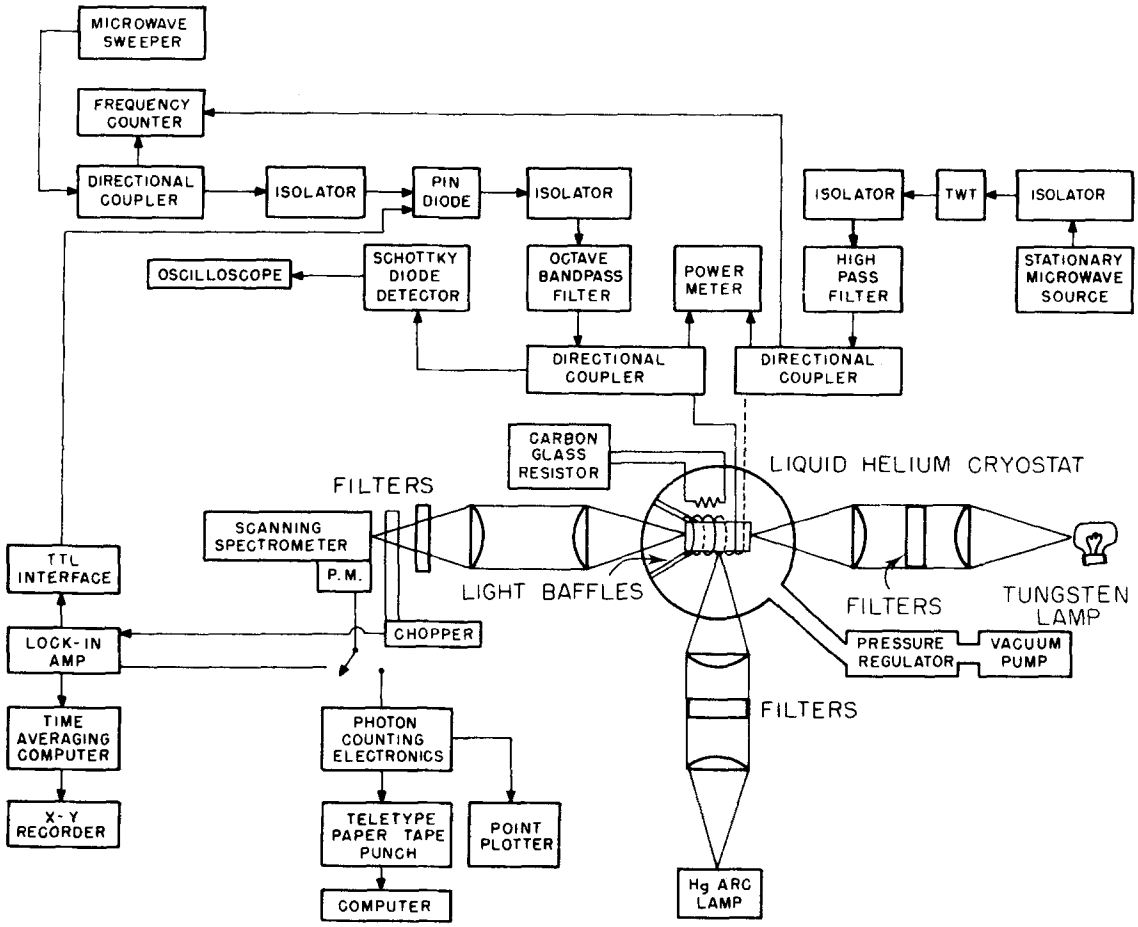

FIG. 1. Block diagram of the low temperature optical and magnetic resonance spectrometer used in the experiments.

ergy localization in these organic crystals and it should be recognized that statements in the text may only apply to such crystals.

II. EXPERIMENTAL

A simplified schematic of the optical and magnetic resonance spectrometer used in these experiments is shown in Fig. 1. The spectrometer was used for optically detected magnetic resonance (ODMR), phosphorescence microwave double resonance (PMDR), microwave-optical hole burning, optical emission, and optical absorption experiments. In what follows we divide the experimental procedure and apparatus into four categories—samples, cryogenics, optical detection and data processing, and microwave electronics.

A. Samples

Raw perprotophenazine, (9, 10-diazaanthracene, $C_{12}H_8N_2$) was obtained from the Aldrich Chemical Company and purified by extensive zone refining under oxygen-free conditions. Perdeuterophenazine ($C_{12}D_8N_2$) was obtained from Merck, Sharp and Dohme of Canada, Ltd. and subsequently zone refined. Mass spectroscopic analysis showed the deuterophenazine to be better than 98% isotopically pure. Mixed single crystals of proto in deuterophenazine were grown in small and large temperature gradient Bridgman furnaces ($\frac{1}{2}$°K/15 cm and 5°K/cm, respectively) under oxygen free conditions. After growth the mixed crystals were analyzed on a mass spectrometer, yielding the mole fractions of deuterated, partially deuterated, and protonated phenazine present in each sample. For reproducibility, several mass spectra of each crystal were run and the statistically averaged results are presented in Table I. Care was taken to use a low ionizing voltage (~10 eV) and low source pressure ($\sim 2\times10^{-7}$ Torr) yielding a typical ion current of 6×10^{-8} A to minimize isotopic exchange and fragmentation effects (in particular, those dissociations yielding parent ions minus one hydrogen or deuterium). Even with these low ionization voltages we have found some differences in the analysis.

TABLE I. Mole percentage isotopic composition of mixed phenazine crystals.

Crystal	$C_{12}H_8N_2$	D_6	D_7	$C_{12}D_8N_2$
1[a]	0.6±0.1	2.0±0.2	17.3±0.2	80.0±0.2
2	2.0±0.1	4.0±0.3	17.1±0.7	76.9±1.0
3	3.0±0.2	3.5±0.2	16.7±0.4	76.8±0.4
4	4.44±0.02	3.4±0.2	17.2±0.1	76.0±2.0
5	5.65±0.06	1.8±0.1	16.7±0.2	76.0±0.2

[a]Only one mass spectrum was available, so statistically averaged results are not possible. Errors estimated (very generously) from peak heights.

TABLE II. Mole percentage isotopic composition of mixed DBN crystals.

Crystal	$C_{10}H_6Br_2$	D_4H_2	D_5H_1	$C_{10}D_6Br_2$
1	≤0.3	0.6±0.2	10.2	88.9
2	2.9	0.3±0.3	10.5	86.3
3	4.8	0.3±0.3	9.7	85.2
4	8.2	0.2±0.2	8.7	82.9
5	11.9	0.2±0.3	8.6	79.3
6	14.5	1.1±0.5	11.5	72.9
7	21.8	<1	7.7	70.5
8	24.1	<1	7.1	68.5

Raw perproto 1, 4-dibromonaphthalene (DBN), $C_{10}H_6Br_2$, was obtained from Eastman Chemical Company, raw perdeuterated 1, 4-dibromonaphthalene, $C_{10}D_6Br_2$, from Merck, Sharp, and Dohme of Canada, Ltd. Proto and deutero DBN were purified by extensive zone melting. Isotopically mixed crystals were grown, again by standard Bridgman techniques. The isotopic composition of the mixed crystals, as determined by the mass spectrometric analysis of Merck, Sharp, and Dohme, is shown in Table II. Throughout the paper, we will refer to the crystals by the percentage of the perproto species present.

The samples were cooled slowly from room temperature to 77°K in a helium atmosphere over ~6 h. No fracturing of crystals was visible at that point. The crystals were then cooled to 4.2°K by the transfer of liquid helium into the cryostat, still no fracturing observable. Care was taken so as not to allow the crystals to warm up between subsequent liquid helium transfers, as rapid thermal cycling over large temperature ranges may affect the strain broadening of the crystals, which in turn might affect the transport dynamics under study. In addition, while making temperature dependent measurements, care was taken to allow the crystals a minimum of 7 min to come to thermal equilibration with the helium bath (while irradiating with the light source). We have observed while doing temperature-dependent measurements on phenazine-d_8 in superfluid helium, that equilibration times much less than 5 min give irreproducible emission intensities for temperature changes of ~0.8°K. Equilibration times should in principle be longer for the low temperature measurements as the Kapitza contact resistance[9] goes roughly as T^{-3} (and increases with the number of asperities on the sample surface). We did not make detailed measurements of equilibration times, yet we wish to bring attention to this potential source of error. Further, for temperatures close to but below the lambda point, we have observed local boiling of the superfluid on the surface of the light baffles, which implies sample heating may also occur (keep in mind that for T greater than 1°K, He II will not support temperature gradients).

Our measurements were tested for equilibration by finishing the temperature run (say, ending at high temperature) then redoing the initial measurement (low temperature) using a temperature sensor near the crystal. When equilibration was complete, excellent agreement was found. For the magnetic resonance experiments and most optical experiments the samples were mounted in as strain-free a manner as was possible by placing the crystals within a helix and supporting the crystals from beneath with tape. (The weight of the crystal on itself and the hydrostatic pressure of the helium bath which changes during the experiment may contribute to the crystal strain.) For the experiment in which the trap depth and temperature dependent emission intensity were measured, the samples were gently taped into a sample compartment (which was attached to light baffles) using black photographic tape. In these experiments all crystals were mounted on the same holder which has large open windows to insure helium circulation around the crystals.

B. Cryogenics

The sample holder was immersed in a metal dewar. The temperature of the helium bath was regulated to ±5 mK between 4.2 and 1.12°K. For temperatures above 1.6°K, regulation was achieved with a Lakeshore Cryotronics model 329 vacuum regulator. For all but one experiment, helium reservoir temperatures were measured with a calibrated carbon glass resistor to ±5 mK. The immersion thermometer was placed as close as was practical to the samples (≤30 mm). For one experiment (the temperature dependence of the emission intensity for the 2% h_8/d_8 phenazine) the crystal temperature was measured by vapor pressure thermometry, which reproduced the earlier results for the dimer to monomer ratio measured by the carbon glass resistor within 4%.

C. Optical detection and data processing

Light from the samples was dispersed with a 0.5 m Ebert mount scanning spectrometer and detected with an EMI 9659QB photomultiplier tube enclosed in a cooled housing. For the optical absorption and emission experiments the slits were held constant at 20 μ by 10 mm unless otherwise noted. The 20μ×10 mm slits yielded a spectral resolution of approximately 0.32 Å at 6470 Å. To reduce the scattered light within the spectrometer, sharp-cut filters passing only long wavelengths were placed directly in front of the entrance slit. All emission and absorption spectra are unpolarized and uncorrected for instrument response. Appropriate solution filters were used to absorb unwanted visible and IR radiation from the 1 kW tungsten lamp or an Oriel 200 W Hg arc lamp.

Phenazine optical spectra were obtained by chopping the luminescence. The chopped luminescence was phase sensitively detected at 100 or 975 Hz and the signal fed to a Varian C-1024 time averaging computer. The spectrum was averaged, if necessary, and plotted on an XY or strip chart recorder. The phenazine spectrum was calibrated by placing an Fe–Ne hollow cathode lamp (20 mA current) directly in front of the spectrometer entrance slit. *Without* interrupting the scan, the calibration lamp was then removed from optical path and the absorption or emission line was recorded. The scan still uninterrupted, the calibration lamp was reinserted in the optical path and the second calibration line was recorded.

Absorption and emission experiments used to determine the trap depth were done on the same crystal at the same temperature without moving the sample in order to insure against artifacts.

DBN emission spectra were obtained with a Nuclear Data series 2200 photon counting system. A hard copy of the digitized spectrum was recorded on HP 7590C point plotter. Using a nonlinear regression computer program, the emission spectra were fit as the sum of Gaussian line shapes. The phenazine emission spectra were digitized by hand and the line shapes were fit in a similar manner. Details of the line shape analysis and results are in Sec. III.

D. Microwave electronics

Samples for the low temperature magnetic resonance experiments were held within a German silver helix wound to dimensions slightly smaller than the lowest order transverse mode. The helix was connected only to the silver plated center conductor of a chrome-plated semirigid coaxial cable, the last two windings being shorted. For the microwave-optical hole-burning experiment, concentric helices separated by a 1 mm thick wall quartz cylinder were used. We did not control the inductive coupling of the helices. The microwaves were square-wave amplitude-modulated to a depth of ≥ 40 dB with Narda 411DJ201 PIN diodes. The square wave for the modulation was derived from the sine wave reference of the lock-in amplifier via a homemade comparator circuit used as a Schmitt trigger. Swept, leveled (± 1 dB) microwaves were supplied by a HP 8620C oscillator with appropriate RF plug ins. The stationary microwave source was a HP 616A reflex Klystron oscillator which was amplified by a Hughes model 1277H (specially selected) 60 W traveling wave tube amplifier, appropriately filtered and isolated. Isolators were used on both sides of the PIN diode to protect the sweeper's YIG oscillator and prevent unwanted reflections. The modulated output of the diodes was passed through an octave bandpass filter. Microwave power incident on the helix was measured by use of a HP 430B power meter connected to a directional coupler situated directly on top of the experimental dewar.

III. RESULTS

A. Phenazine and DBN crystalline structure and intermolecular interactions

Phenazine crystals grown from the melt are of the monoclinic α form[10] with space group $P2_1/a$, two molecules per unit cell. At room temperature, the unit cell has the dimensions $a = 13.22 \pm 0.01$, $b = 5.061 \pm 0.005$, $c = 7.088 \pm 0.007$ Å, $\beta = 109°13' \pm 15'$. The most salient feature of the crystal structure is chains of plane parallel packed phenazine molecules at 45° with respect to the short axis, b. Neighboring chains in the ab plane have their long molecular axes perpendicular to one another (shown clearly in Fig. 2). As we shall discuss later, intermolecular interactions are highly anisotropic for the $^3\pi\pi^*$ band, with b-axis coupling dominating at 6.5 cm^{-1},[11] ab-plane interchange equivalent-pair interaction energy of 0.5 cm^{-1},[12] and coupling along the c axis being immeasurably small by conventional optical techniques. (The 6 cm^{-1} value was obtained after correcting for guest–host interactions.) Thus, one obtains essentially a two-dimensional topology in the ab plane that resembles that of naphthalene.

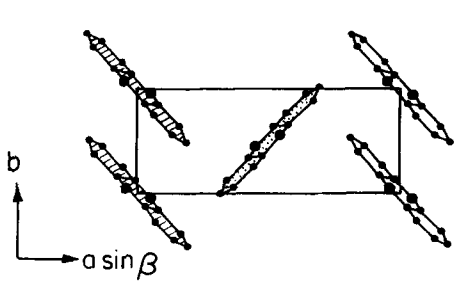

FIG. 2. Projection of the contents of the phenazine unit cell onto a plane perpendicular to the c axis.[10]

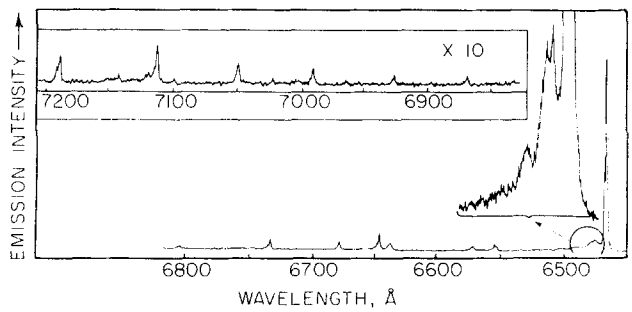

FIG. 3. Vibronic emission spectrum of 2% h_8 in d_8 phenazine at 1.6 °K. From 6820 to 7200 Å the sensitivity has been increased by a factor of 10. The inset shows the side-band spectra at higher sensitivity to reveal the structure. Correction for phototube response would enhance the low energy lines relative to the vibrational origin. The scan is only of moderate sensitivity, making it difficult to see the 4.4 cm^{-1} splitting that occurs on a large number of the vibrational lines (however, see Table III and Fig. 4).

DBN crystallizes[13] in a $P2_1/a(C_{2h}^5)$ space group, 8 molecules per unit cell. Crystallographic axes $a = 27.45 \pm 0.08$, $b = 16.12 \pm 0.04$, $c = 4.09 \pm 0.01$ Å, $\beta = 91°51' \pm 10'$.

The spectra of DBN neat[14] and isotopically mixed[15] exhibit the characteristics of a linear chain with nearest-neighbor interaction of 6.2 cm^{-1}.[15]

B. Vibronic emission spectrum of isotopically mixed phenazine

The unpolarized vibronic emission spectrum of the isotopically mixed single crystal 2% proto in deutero phenazine is shown in Fig. 3. The relative intensities, wavelengths, reciprocal wavelengths (corrected to vacuum) and energy splittings in cm^{-1} are recorded in Table III. The sample was optically excited by a 200 W mercury arc lamp filtered to a passband from 3050 to 4700 Å. Spectral resolution of approximately 20 000 was used.

We record the (0, 0) origin of the proto monomer to be at 15 453 $\pm$ 3 cm^{-1}, whereas the neat phenazine crystal absorption has Davydov components at 15 448 and 15 452 cm^{-1}.[12] With trap states as shallow as in the isotopi-

TABLE III. Analysis of the phosphorescence ($^3B_{2u} \rightarrow {}^1A_g$) of 2% proto in deutero phenazine at 1.6 °K.

Wavelength[a] (Å)	E/hc (cm^{-1}) (vacuum) ± 3 cm^{-1}	Relative[b] intensities	$\delta\tilde{\nu}$ (cm^{-1})	Possible assignment and activity[c]
6468.58	15455.1	vs	M_{00}	monomer origin
6470.24	15451.1	vs	D_{00}	dimer origin
6477.61	15433.5	s	$M_{00}-21.6$	NA, NR
6480.27	15427.2	s	$M_{00}-27.9$	NA, NR [16]
6491.09	15401.5	w	$M_{00}-53.6$	NA, NR
6554.51	15252.5	w	$M_{00}-202.6$	O, NA
6556.50	15247.8	m	$D_{00}-203.3$	O, NA
6573.98	15207.3	w	$M_{00}-247.8$	O, NA
6638.56	15059.3	w	$M_{00}-395.8$	NR, NA
6645.72	15043.1	s	$M_{00}-412.0$	417 (R)
6647.55	15039.0	m	$D_{00}-412.2$	417 (R)
6681.67	14962.2	m	$M_{00}-492.9$	474 (IR)
6683.5	14958.1	w	$D_{00}-493.0$	474 (IR)
6734.77	14844.2	s	$M_{00}-610.9$	612 (R)
6736.43	14840.6	w	$D_{00}-610.5$	612 (R)
6805.01	14691.0	w	$M_{00}-764.1$	751 (IR)
6807.34	14686.0	w	$D_{00}-765.1$	751 (IR)
6871.09	14549.7	vw	$M_{00}-905.4$	902 (IR)
6927.85	14430.5	vw	$M_{00}-1024.6$	1011 (R)
6991.44	14299.3	w	$M_{00}-1155.8$	1156 R(IR)
6993.60	14294.8	vw	$D_{00}-1156.3$	1156 R(IR)
7050.86	14178.8	w	$M_{00}-1276.3$	1279 (R)
7114.28	14052.4	w	$M_{00}-1402.7$	1404 (R)
7116.27	14048.4	w	$D_{00}-1402.7$	1404 (R)
7120.77	14039.6	vw	$M_{00}-1415.5$	NR, NA
7122.93	14035.3	vw	$D_{00}-1415.8$	NR, NA
7143.74	13994.4	vw	$M_{00}-1460.7$	1475 (R)
7190.51	13903.4	w	$M_{00}-1551.7$	1554 (R)
7192.84	13898.7	w	$M_{00}-1552.4$	1554 (R)

[a]The numbers quoted in this table are no more accurate than ± 3 cm^{-1} and therefore the decimals do not reflect high accuracy (see also Table IV).
[b]> 10 very strong, 7–10 strong, 4–7 medium, 1–4 weak, < 1 very weak.
[c]See Refs. 17 and 18. NA = not assigned, NR = not reported, O = observed.

cally mixed phenazine crystal, significant host-band mixing will be present and, as a consequence, the energies of trap and host states are influenced and the dimer and monomer may borrow different amounts of oscillator strength from the host band.

When the signal-to-noise ratio permitted, an average splitting of 4.2 cm^{-1} (standard deviation 0.3 cm^{-1}) was observed in most emission lines. The structure at 21, 27, and 54 cm^{-1} to lower energy from the (0, 0) origin has not been positively assigned.[16]

The vibronic line intensities decrease as one goes to lower energy, yielding a Franck–Condon envelope in rough agreement with other work.[17] The observed average monomer–dimer splitting of 4.2 cm^{-1} for all lines agrees well with the splitting of 4.4 cm^{-1} ± 0.5 cm^{-1} from the work of Zewail[11,19] and the high resolution computer fit data described later in this work. In the emission spectrum to the vibrational levels of the ground electronic state, one would expect to see the 4.2 cm^{-1} splitting on all lines only if the ground state vibrational splittings were small and the line broadenings were negligible. If the vibrational splittings were considerable compared to the excited state splitting, the 4.2 cm^{-1} splitting might be altered and for the case of dimer emission, new selection rules for optical emission would likely be involved. One can conclude then, for most vibronic lines of the phenazine emission that ground state splitting is relatively small.

The ratio of the dimer to monomer emission intensity (D/M), within experimental error, appears to be the same for all relevant vibronic lines.[20] For example, for the (0, 412) transition, the D/M intensity ratio is 0.45 ± 0.03 compared to 0.50 ± 0.02 for the (0, 0) origin, with splittings of 4.0 and 4.1 cm^{-1} (within our resolution), respectively. The (0, 412) transition and (0, 0) transition at 1.6 °K are shown in Fig. 4. At this temperature and from the impurity emission spectrum of the 2% crystal, we also obtain an optical Debye–Waller factor[21] of 0.2 to 0.25, as measured by use of a polar planimeter averaged for several different spectra. An insert, showing the detailed structure of the phonon sideband is depicted in Fig. 3.

Spectroscopic trap depths were measured for the 0.5% and 6.6% h_8 in d_8 phenazine crystals at 1.36 °K. Measurement of absorption spectra for the two crystals yielded the Davydov splitting of the host band. Measurement of the emission spectrum of the 0.5% and 6.6% crystals yielded the trap depths of the monomer and dimer, respectively. The measurements indicate: (1) a trap depth in the 0.5% crystal of 23 ± 2 cm^{-1} from the

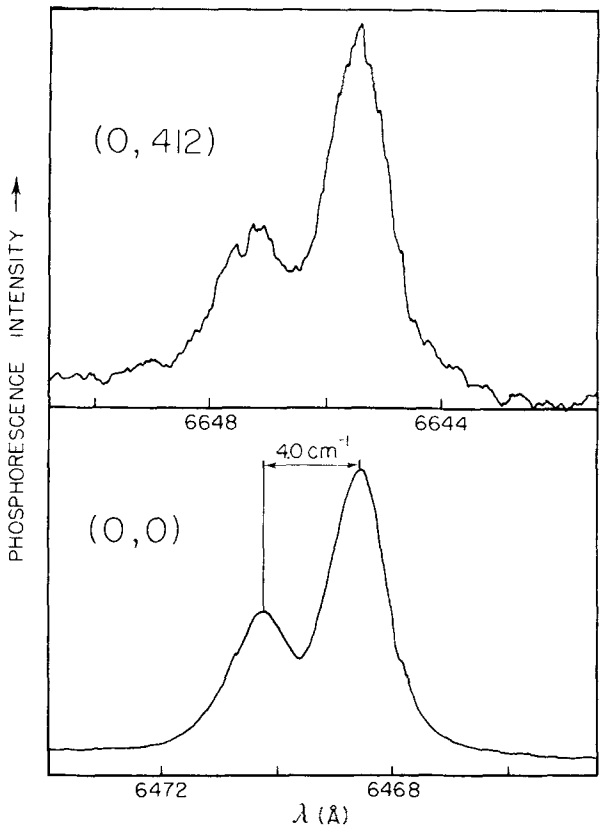

FIG. 4. Monomer and dimer emission lines for the 412 cm^{-1} molecular vibrational mode and the vibrational origin of the 2% phenazine crystal at 1.6 K. Relative intensities of the vibrational lines may be seen in Fig. 3. The gently sloping baseline that increases to lower energy is present in 412 cm^{-1} *vibronic* line and the (0, 0) origin.

TABLE IV. Emission (E) and absorption (A) spectra of pure and doped phenazine crystals.

Crystal %h_8	T(K)	$\bar{\lambda}$(cm^{-1})[b]	Assignment		Investigators
6.6	1.36	15477.8 15474.1	Davydov doublet	(A)	This work
		15447.6	dimer & trimer	(E)	This work
0.5	1.36	15477.9 15474.3	Davydov doublet	(A)	This work
		15453.2	monomer trap	(E)	This work
pure D	4.2	15467 15471	Davydov doublet	(A)	Clarke and Hochstrasser[a]
pure H	4.2	15448 15452	Davydov doublet	(A)	Clarke and Hochstrasser[a]

[a]See Ref. 12.

[b]The values we report are *in vacuo* and are regarded to be accurate to ± 3 cm^{-1}. The values of Clarke and Hochstrasser are possibly in air (private communication) and for the deutero Davydov states differ from our measurements by 4.6 Å. Note that the trap depth of the 6.6% (Fig. 5) can be corrected for the dimer and trimer emission to yield a monomer trap depth of 22 cm^{-1}, which is in excellent agreement with the 0.5% result (23 cm^{-1}). Our numbers for the absorption measurement in this table and the emission measurement (0, 0) in Table III agree with those of Doberer, Port, and Wolf.[64]

middle of the host deutero $k=0$ bands to the "isolated" proto impurity; (2) a possible weak dependence of the trap depth on dopant concentration, since there is a 1.6 cm^{-1} red shift between the dimer in the 6.6% crystal from where one might expect it from the 0.5% measurements. However, this shift is due in part to the emission of trimer aggregates building a shoulder upon the true dimer emission, and is within our experimental error; and (3) a Davydov splitting of 4 cm^{-1} for the deutero host which contains impurity band states in good agreement with earlier work.[12] These results, together with other measurements are compiled in Table IV. The calibrated absorption and emission spectra for the 6.6% crystal are shown in Fig. 5 with an insert to show the Davydov doublet more clearly.

For DBN, the optical spectroscopic properties have been well characterized[14,15] and when applicable our

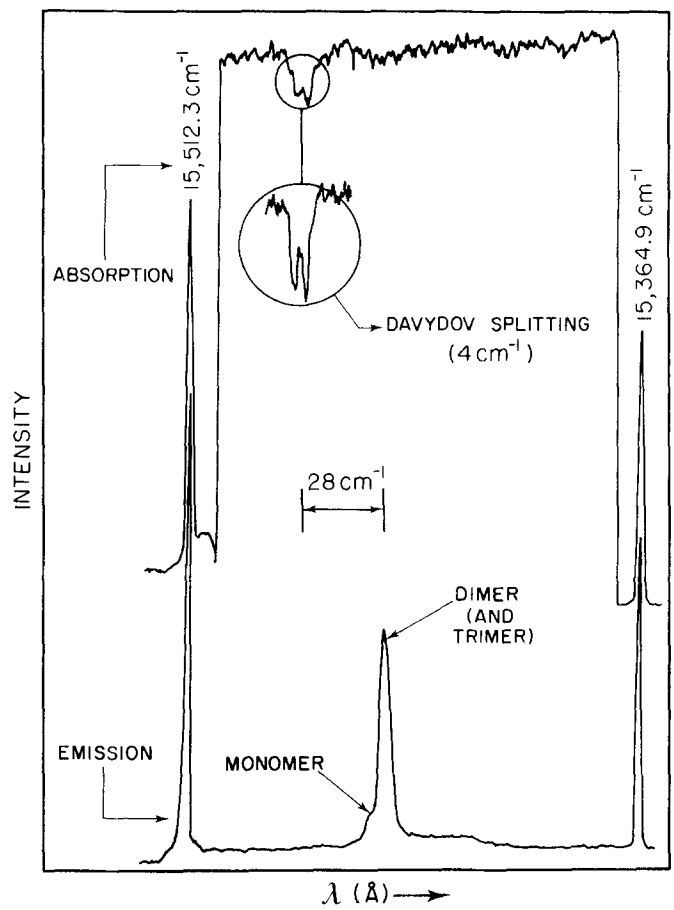

FIG. 5. Superimposed absorption and emission spectra of a 6.6% phenazine at 1.36 °K calibrated by standard neon lines at 15 364.9 and 15 512.3 cm^{-1}. The Davydov doublet is shown at higher resolution in the inset in the figure. The emission in the spectrum is dominated by the dimer and trimer, since at 1.36 °K the deeper traps acquire the majority of the population. The 28 cm^{-1} measured from the middle of the Davydov doublet to the peak of the trap emission is not the true trap depth of any cluster. Computer fit of the emission yields 22 cm^{-1} as the energy difference between the middle of the two $k=0$ states and the monomer which is within experimental error of the 0.5% results. Note that the Davydov doublet in the 6.6% crystal is still clearly resolved. The 6.6% crystal was 5 mm thick.

measurements agree well with previous work dealing with monomer–dimer–trimer splittings.

C. Effect of guest concentration on emission spectra

The observation of abrupt changes in intercluster energy transfer rates for phenazine and DBN was accomplished by comparing the populations of different impurity clusters (monomers and dimers) as a function of dopant concentration and sample temperature. In this section we present the experimentally measured trap emission intensities (energy resolved) as a function of impurity concentration.

Figure 6 shows the dimer to monomer emission intensity ratio as a function of concentration for phenazine, presenting new data in addition to those shown in earlier work by us.[5] The dimer and monomer emission intensities in Fig. 6 are the integrated peak areas as fit by a computer generated line shape function (see Fig. 7). Due to splittings that are small in comparison to the broadening, it is reasonable to fit the emission line shape only to monomer, dimer, and to some extent, trimer. Emission from translationally inequivalent dimers, translationally equivalent monomers separated by one host molecule (double monomer), and other more complex impurity clusters can be compensated for *a posteriori*, but their precise position and linewidths cannot be extracted with certainty from the measurements herein alone.

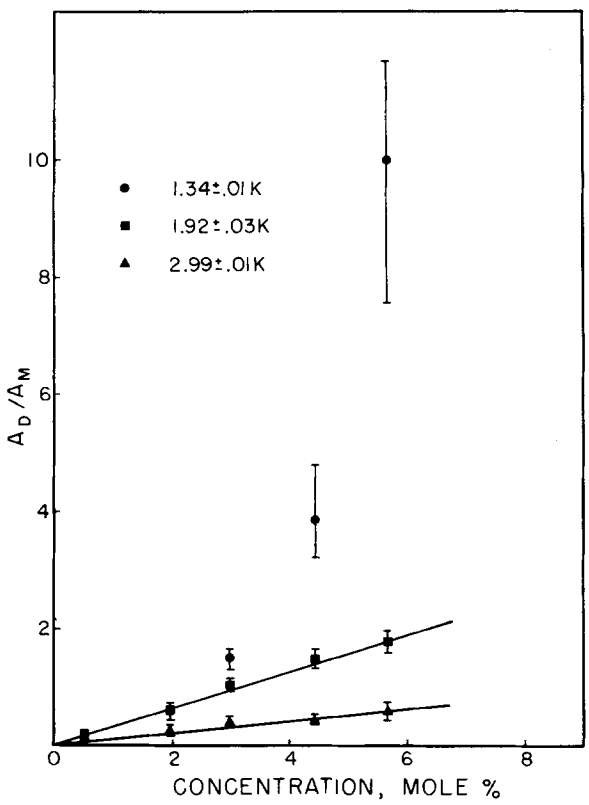

FIG. 6. The computer fit (integrated peak area) dimer/monomer phosphorescence intensity ratio as a function of proto trap concentration for 1.92 and 1.34 °K. The data for 2.99 °K are from peak heights, as the signal/noise was insufficient to permit reliable computer analysis. For the computer fits, the error bars are those determined by the nonlinear regression and represent 80% confidence limits of a 5 degree of freedom double-tailed student "t" statistic (see e.g.[61]). The new data agree within error with the data published previously.[5] The crystal concentrations are those of a statistically averaged mass spectral analysis (see Table I). The data for 1.92 and 2.99 °K yield very nearly straight lines and were fit by linear least squares to yield $D/M = 0.02 + 0.36C$ ($\sigma = 0.06$) and $D/M = 0.09 + 0.12C$ ($\sigma = 0.07$), respectively.

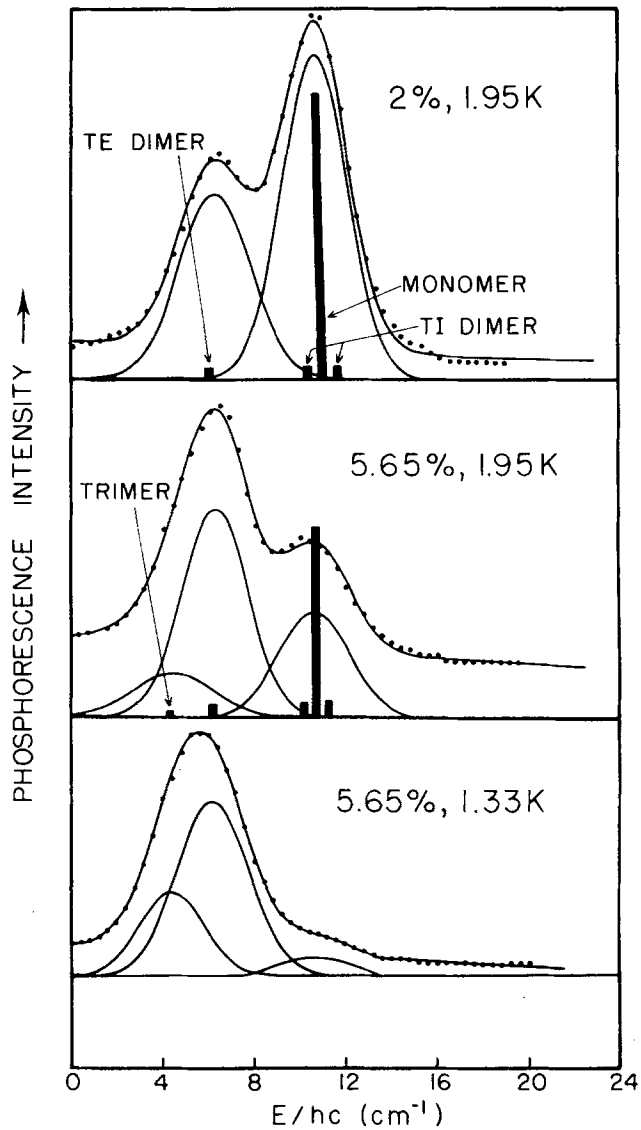

FIG. 7. Examples of computer optimized line shape fits (smooth lines) of the data (dots) for the vibrational origin of 2% and 5.65% phenazine. Only the relative energies of the fitted peaks are shown as absolute values and listed in Table III. The histogram bars superimposed on the emission spectra are the relative statistical probabilities for each cluster (see section on cluster statistics). The fit for the sloping base line is not shown to avoid confusion in the figure. However, one can see the slope is greater for the 5.65% crystal than the 2% crystal.

The trap emission envelope was fit as the sum of a straight baseline and Gaussian line shapes for the monomer, dimer, and trimer (if present). In principle, each cluster emission envelope should have a phonon sideband of its own. Thus, the monomer sideband will contribute more to the baseline offset of the dimer than the mono-

TABLE V. Computer fit inhomogeneous linewidths of cluster emission in mixed phenazine crystals.

Protoisotopic Conc., mole%	T (K)	$FWHM^{a}_{monomer}$ $(cm^{-1})^{c}$	$FWHM^{b}_{dimer}$ $(cm^{-1})^{c}$	$FWHM_{trimer}$ $(cm^{-1})^{c}$
0.6	1.92	2.6±0.1	3.6±0.8	
2.0		3.4±0.1	3.8±0.2	
3.0		3.3	3.7	
4.44		3.1±0.2	3.1±0.1	
5.65		3.6±0.3	3.4±0.1	4.0±0.8
0.6	1.34	2.8±0.1	3.5±0.8	
2.0		4.0±0.1	4.0±0.2	
3.0		3.7±0.3	3.8±0.2	
4.44		2.7±0.3	3.1±0.1	
5.65		3.4±0.6	3.7±0.1	3.2±0.2

[a]Average $FWHM_{monomer} = 3.26\ cm^{-1}$; $\sigma = 0.46$ (14% standard error)
[b]Average $FWHM_{dimer} = 3.57\ cm^{-1}$; $\sigma = 0.31$ (9% standard error).
[c]All error bars are from 80% confidence interval.[61]

mer emission. We make the approximation that the sum of the sidebands results in a linear sloping baseline for all trap emission. No noticeable change in slope over the temperature range from 1.3 to 3 °K was observed. However, there was a slight increase in baseline slope with increasing dopant concentration.

Using the computer fits, the monomer–dimer splitting was experimentally determined in the 2% h_8 in d_8 phenazine crystal at 1.33 °K to be 4.4 cm^{-1}. The 2% crystal was chosen for the determination of the resonance splitting so that in the computer fit of the data, trimer emission would be negligible and use of two Gaussians whose FWHM, amplitude, and center were parameters would produce a fit which is most nearly correct. Further, the low temperature spectrum was chosen since the S/N ratio increases as the sample temperature decreases (see Sec. D on the effects of temperature). The

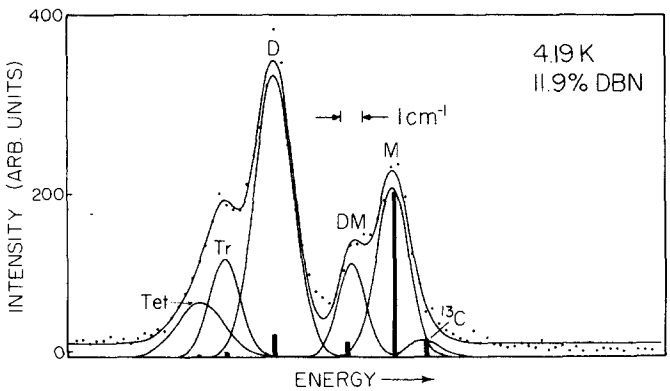

FIG. 8. Computer fit (smooth line) of data (dots) for 11.9% DBN at 4.19 °K. Legend: ^{13}C = carbon 13 monomer, M = monomer, DM = double monomer, D = dimer, Tr = trimer, Tet = tetramer. Histogram bars indicate relative cluster probability from the exact results of Sec. IVA. The monomer–dimer splitting was variable in the computer fit from which the dimer–trimer and trimer-tetramer splittings were *fixed*. The double dimer was not included in the fit due to the vanishing statistical probability of occurrence. All peaks' FWHM and height were variable in the fits. In all cases, the $^{13}C/^{12}C$ monomer emission intensity ratio was that expected by isotopic abundance, i.e., 11% (within the error bars).

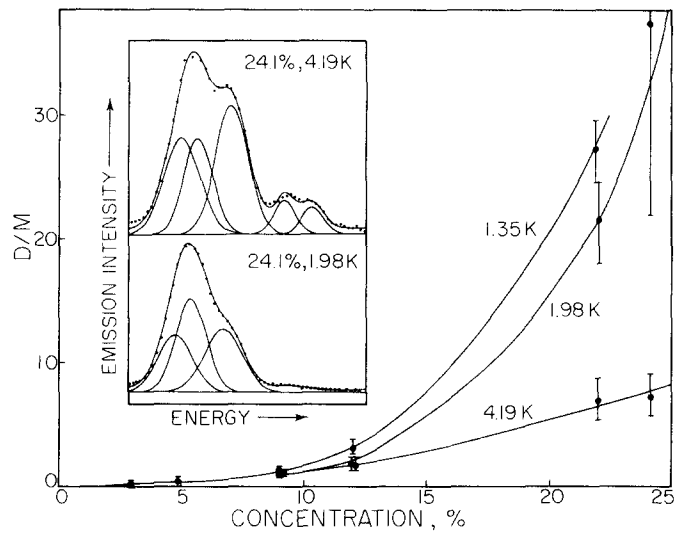

FIG. 9. The computer fit areas for the dimer/monomer emission intensity ratio for DBN as a function of temperature and concentration. Observe the "sluggishness" of the threshold behavior in this quasi-1-D system as compared with phenazine (Fig. 6). This is due in part to the fact that the superexchange coupling scales exponentially as c^{-1} for 1-D and $c^{-1/2}$ for 2-D (see Sec. VIA). The uncertainty in D/M for the 21.8 and 24.1% crystals results from the congestion of cluster emission lines and reflect approximately 70% confidence limits. However, from the inset for the 24.1% case, it is clear that D/M changes considerably. In the low temperature fit, peak positions from the high temperature fit were used to locate the dimer, trimer and tetramer. For low concentrations, when only one point is shown, the D/M ratios for all three temperatures coincide well within the error bar. In the insert, the 24.1%, 4.2 K spectrum shows the "quasi-Boltzmann" behavior (see Fig. 11) of the D/M ratio: $2(0.24)\exp(5.5/4.2\times0.69)$. For the trimer and tetramer the errors on the intensities from the computer fit are quite large due to the absence of (apparent) splitting. At lower temperature we do not expect this quasithermal behavior to hold. The results of the 14.5% of Ref. 15 fits smoothly with our curves.

4.4 cm^{-1} splitting was then used as a fixed parameter in the remainder of the computer generated fits. The linewidths from the 2% crystal analysis were not useful in fitting other crystal spectra, likely due to the difference in strain broadening from sample to sample (see Table V) or due to intrinsic correlation effects that are a function of concentration. However, no obvious trend for the linewidths as a function of concentration was found. For the 5.65% crystal the dimer–trimer splitting was a fixed parameter (from knowledge of the monomer–dimer splitting) and trimer amplitude and FWHM where variable. Examples of computer fits are shown in Figs. 7 and 8 for phenazine and DBN, respectively.

In I, we used peak heights for calculating D/M. Here, if we used the integrated areas *with* and *without* the trimer the D/M ratio is still within our error. The small but noticeable broadening and shift of the dimer line to lower energy for the 5.65% crystal as the temperature is reduced is due to trimer population increasing as the temperature is lowered, which is shown clearly in the computer fits of Fig. 7. If one attempts to fit the 1.33 °K data for the 5.65% crystal with just two Gaussians (monomer and dimer) one finds splittings in-

consistent with the 4.4 cm^{-1} value for the 2% crystal and an unphysically large FWHM for the dimer peak.

Similarly, the computer fit of DBN emission spectra provided us with the dimer-to-monomer ratio as a function of temperature and concentration. The monomer and dimer are well resolved for the DBN case but the carbon-12 monomer is closely flanked by the carbon 13 monomer and the (presumably) double monomer[15] (DHDHD $\cdots$) such that they form shoulders. Using carbon 13-carbon 12 monomer splitting (1.9 cm^{-1}) from previous high resolution work[15] as a fixed parameter and letting the dimer–monomer splitting and monomer–double monomer splitting be adjustable parameters produced good fits. Furthermore, knowing the monomer–dimer splitting accurately we predicted, for a linear chain, the position of the trimer and tetramer; thus trimer and tetramer positions become fixed parameters. In all cases, peak amplitudes and FWHM were adjustable parameters (see Fig. 8). For comparison of the results

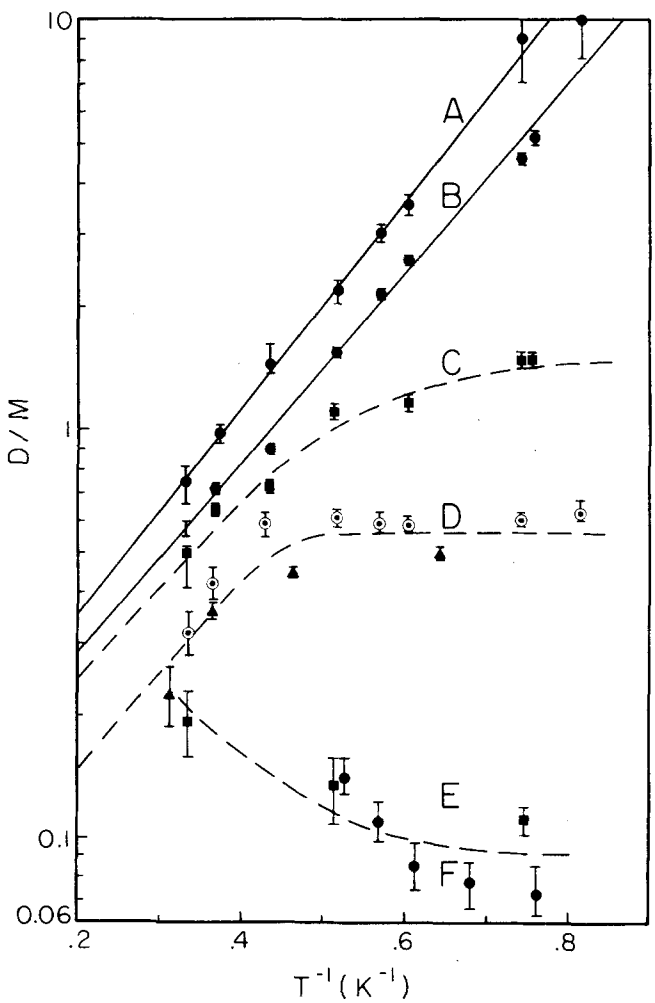

FIG. 10. Plot of log(D/M) vs T^{-1} for (A) 5.65%, (B) 4.4%, (C) 3%, (D) 2%, and (E), and (F) 0.5% h_8 in d_8 phenazine. The D/M ratios are from peak heights. The new data in this plot for the 2% crystal clearly show the "knee" at $T^{-1} = 0.5\ K^{-1}$. In the previous work, signal-to-noise did not permit unequivocal identification of the knee. An asymptotic high temperature activation energy of ~ 4 cm^{-1} is observed for high concentration crystals. When more than one set of symbols appears for a given curve, data were recorded in two entirely different experiments.

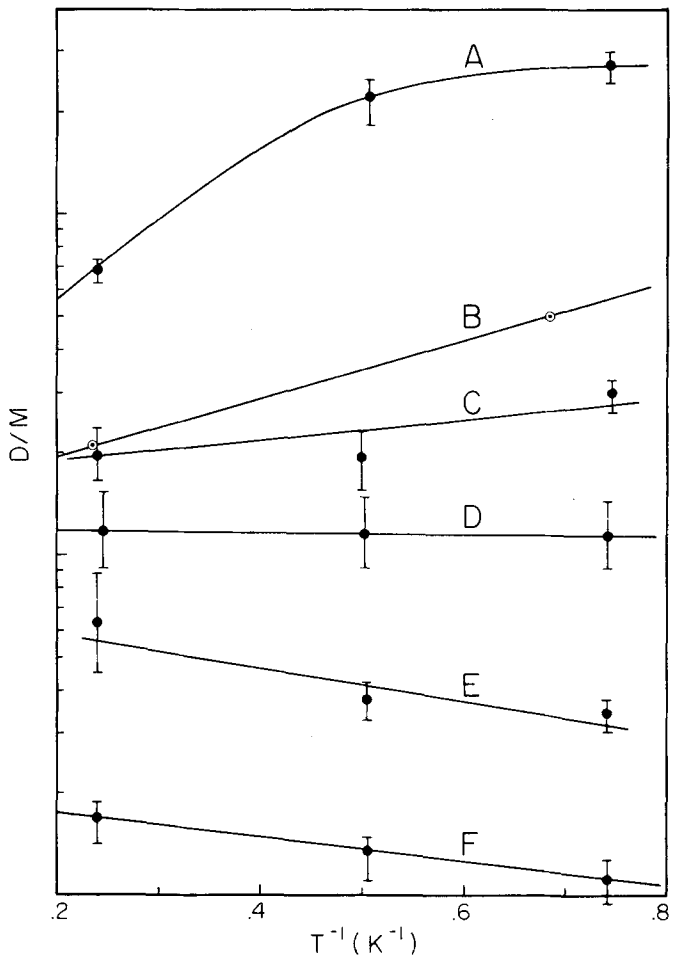

FIG. 11. log(D/M) vs T^{-1} for the following DBN crystals: (A) 21.8% h_6 in d_6, (B) 14.5%, (C) 11.9%, (D) 8.2%, (E) 4.8%, and (F) 2.9%. The dimer was not observed in the 0.1% crystal. The ratios are from computer fits of the experimental data except for the 14.5% crystal which is from peak heights. Curve B was taken from Ref. 15.

of DBN, the quasi-one-dimensional system, with that of phenazine, the quasi-two-dimensional system, we depict the concentration dependence of dimer-to-monomer ratio for DBN in Fig. 9. Again, for DBN as in phenazine, one notices the disappearance of the abrupt change in D/M as the temperature increases. However, this "abrupt" change in D/M occurs at a critical concentration much different in DBN compared to phenazine, a point that we shall discuss in the coming sections.

The error bars for the DBN data are determined by a nonlinear regression routine and are large for high concentrations due to the overlap of dimer, trimer, tetramer emission. Where only one data point is shown for lightly doped crystals, data for all three temperatures coincide well within the error bars. Thus, only one data point is shown to avoid confusion. Comparison of the spectra for DBN at higher concentration at two temperatures can be found in the insert of Fig. 9.

D. Temperature effects

We have measured the temperature dependence of: (1) the dimer/monomer intensity ratio as a function of dopant concentration in phenazine, as shown in Fig. 10

(a portion of the data in Fig. 10 is also present in Fig. 6); (2) dimer/monomer intensity ratio for DBN at various dopant concentrations (Fig. 11); and finally (3) the emission intensity of monomer and dimer trap states for phenazine (Figs. 12 to 15). Again, in all these experiments, the temperature was carefully regulated and measured near the crystal. When S/N permitted, emission intensities and error bars were obtained from computer-analyzed experimental data. In Fig. 10, the 0.5% crystal has two sets of data points. Curve F was taken using the regrown crystal of curve E. The major difference between the samples is presumably the crystal strain; curve F likely to be the less strained of the two, due to the method of preparation and number of thermal cyclings it had undergone.

We mention that for the 0.5% phenazine crystal, temperature dependence of the emission intensity was measured in two independent experiments to demonstrate the reproducibility and to ascertain the largest possible error in the measurement of signals with relatively *much less intensity* (in this case, the dimer). Further, one set of measurements was taken by going up in temperature and the other by going down in temperature. As expected, the experiment demonstrated no temperature dependent hysterisis effects. We note that in this work we did not attempt to make measurements above or near the lambda point of helium in the immersion dewar. This is because, from previous experience, we could not reproduce data at these temperatures, perhaps due to emission scattered by boiling helium or thermal effects that take place in these (molecular) solids.

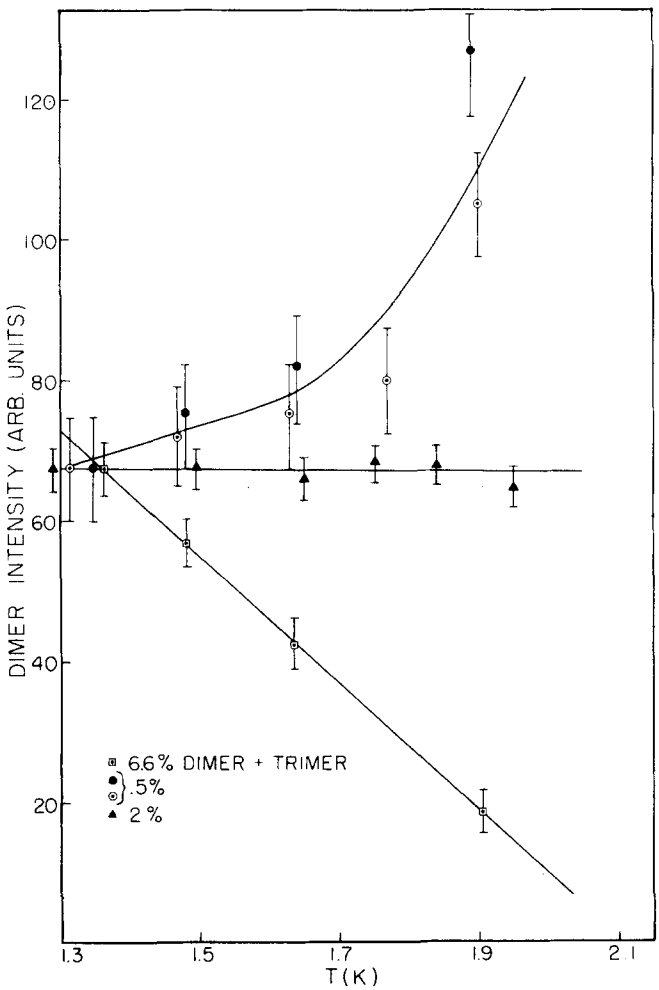

FIG. 12. Normalized emission intensities (peak heights) of the phenazine dimer (or dimer+trimer in the 6.6% crystal) as a function of temperature. The data (and the error bars for each crystal) are multiplied by a constant to make their intensities commensurate at 1.3 °K. The data for the 0.5% crystal show a net increase in dimer population with temperature where the 6.6% crystal has the opposite behavior. These trends indicate indirect and direct communication channels, respectively (see text). The 2% crystal would then represent the ambivalent direct and indirect channels. Where more than one symbol is shown for a given curve, each symbol represents a different experiment.

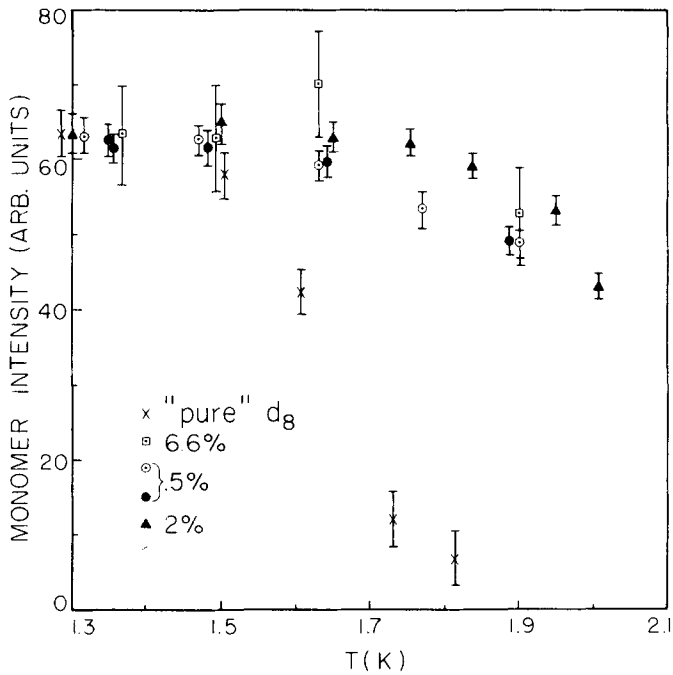

FIG. 13. Phenazine monomer emission intensity as a function of concentration and temperature normalized in the same manner as the data in Fig. 12. In all cases, the intensity decreases (or slightly changes) as temperature increases and is most pronounced in the "pure" d_8 crystal. The pure d_8 crystal shows the loss of population with roughly an 18 cm^{-1} activation energy (see Fig. 14). The remaining crystals all show a similar general trend for loss with no well defined activation energy.

For comparison to the normalized emission intensity vs T plots, we have prepared log of emission intensity vs T^{-1} plots for a "pure" d_8, 0.5%, 2%, and 6.6% crystals. The pure d_8 crystal which contained a vanishingly small amount of proto monomer was chosen in order to have a lattice with monomers as dilute as was possible. The 6.6% crystal was chosen as a sample beyond the critical transition. The 6.6% and pure d_8 crystal were not mass spectrally analyzed, but this was not necessary for the purposes of the emission intensity experiment. The large error bars for the 0.5% and 6.6% crystals are due to the dimer or monomer peak being very small.

E. ODMR, PMDR, and hole burning

The ODMR of the monomer and dimer shows a "central" peak flanked by satellites due to hyperfine split-

tings. The transitions in zero field for the monomer ($D+E=2562.3$ MHz and $2E=640.8$ MHz) are different from those of the monomer (11). The results are consistent with early work on phenazine in a diphenyl host,[22] and also with recent work.[23]

Knowing the frequencies for the monomer and the dimer in the isotopic mixed crystals, we detected the emission of the dimer (or monomer) alone by scanning the total emission in wavelength while the modulated microwave pump was fixed at the frequency of the dimer (or monomer). This high-resolution PMDR method was useful in determining the optical broadening of the dimer.[5]

An example of inhomogeneous broadening in the ODMR spectrum is shown in Fig. 16. To obtain these spectra we have used 60 mW (continuous) microwave power as the swept frequency, chopped at 110 Hz and the stationary field of 125 mW was applied to the outer helix (unchopped) at the frequency indicated in Fig. 16. Better S/N was obtained at lower guest concentrations.

IV. THEORETICAL CONSIDERATIONS

A. Cluster statistics

Given a linear array of N sites randomly occupied by G guests and H hosts, the number q_n of guest clusters

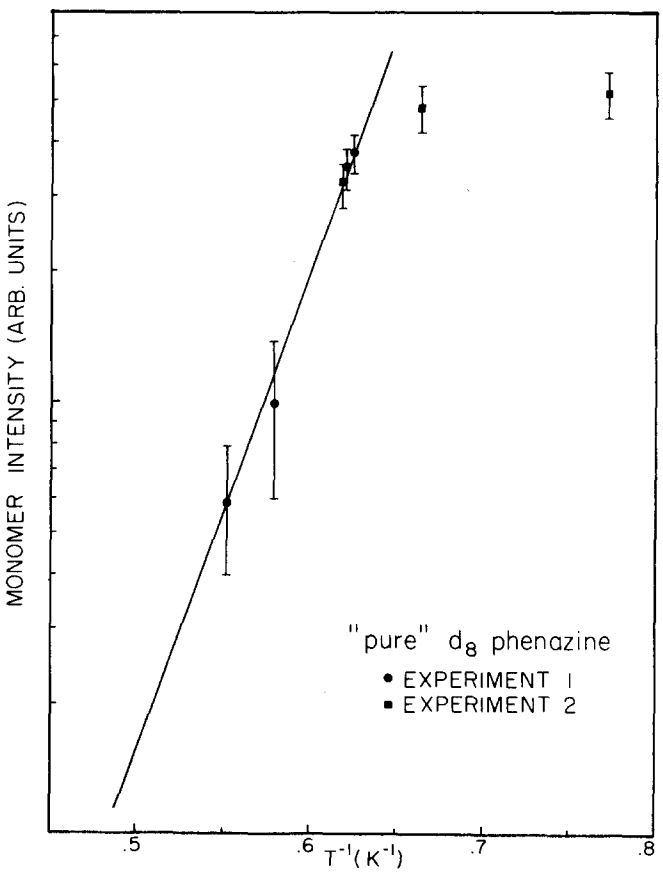

FIG. 14. Arrhenius-type plot for pure d_8 phenazine showing an 18 ± 1 cm^{-1} activation energy (using the 5 data points at highest temperature). Thus we have clear illustration of detrapping most likely to host states. The activation energy differs slightly from the trap depth, most probably due to the presence of states below the host band.

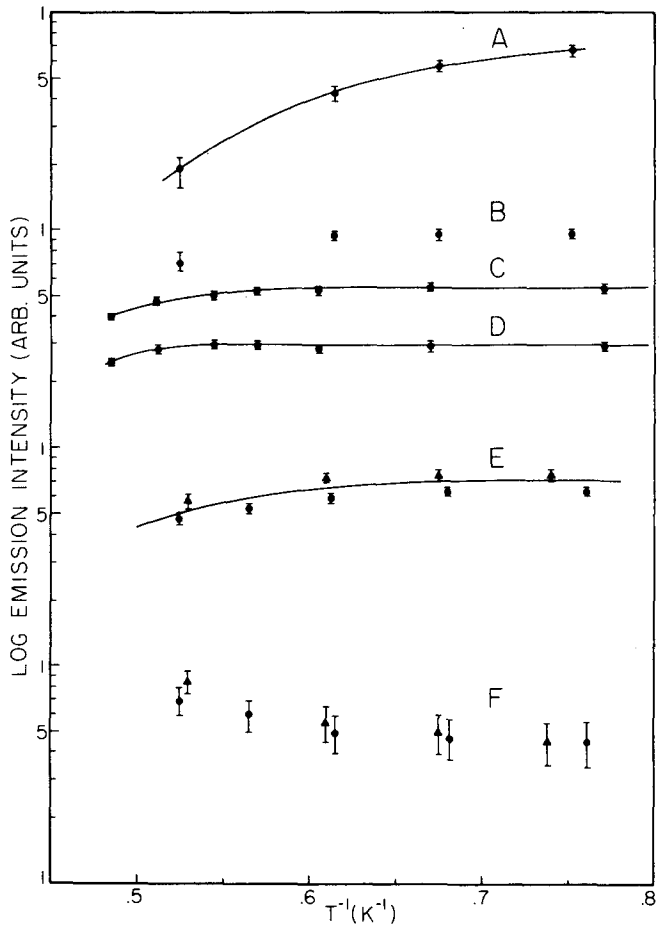

FIG. 15. Activation energy plots of specific cluster (phenazine) emission intensity for the following: A) dimer, 5.65% (B) monomer, 5.65%, (C) monomer, 2%, (D) dimer, 2%, (E) monomer, 0.5%, and (F) dimer, 0.5%.

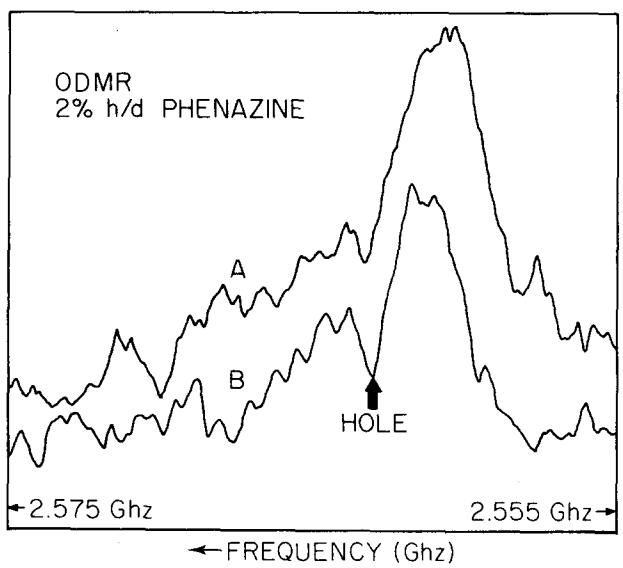

FIG. 16. Hole burning in the ODMR spectrum of 2% h_8 in d_8 phenazine. Spectrum A was taken using 60 mW (cw) microwave power, 1.6 °K. Spectrum B: all conditions *identical* to A, except that a stationary microwave field is applied (125 mW at 2.5635 GHz; arrow marks stationary frequency in diagram). The microwaves were square wave modulated at 110 Hz to a depth of 40 dB. Spectral diffusion may be occurring which would alter the depth and width of the microwave absorption hole. Better S/N are obtained when wide-slit detection is used.

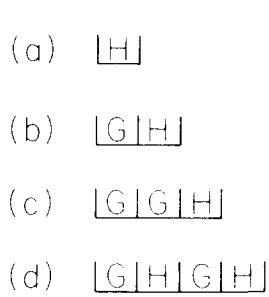

FIG. 17. Guest clusters in 1-D. Each box represents a site in a onedimensional chain which must be occupied by either a guest (G) or a host (H). (a) The single host specie or null culster for $n=0$ (see text for explanation of symbol) which fills sites between guest clusters. (b) the guest monomer, $n=1$. (c) The guest dimer, $n=2$. (d) the "double monomer."

containing n contiguous guests, where $n=0, 1, 2\ldots$ is

$$q_n = N(1-C)^2C^n$$
$$= N(1-G/N)^2(G/N)^n \ . \qquad \text{(IV.1)}$$

Similarly, one can predict in a chain N long, the total number of j contiguous n-mers to be

$$d_{jn} = (N-G-q_n)(1-q_n/N-G)(q_n/N-G)^j \ . \qquad \text{(IV.2)}$$

For $j=2$, $n=1$ one has the so-called "double monomer" whose configuration is shown in Fig. 17.

A linear chain of 10 000 sites was used to model the infinite 1-D lattice. An appropriate number of computer-generated random numbers between 1 and 10 000 were used to populate the lattice with the desired number of impurities. (The computer program must be able to choose another random number in the event that a particular random number is generated more than once. Otherwise, in the process of generating, say, 1000 random numbers, less than 1000 sites may be populated by impurities and this incomplete population will vary in an unpredictable manner from run to run.) An algorithm to count the isolated and multiple contiguous impurity clusters was written and the Monte Carlo results are shown in Fig. 18 for DBN type lattices (one dimensional).

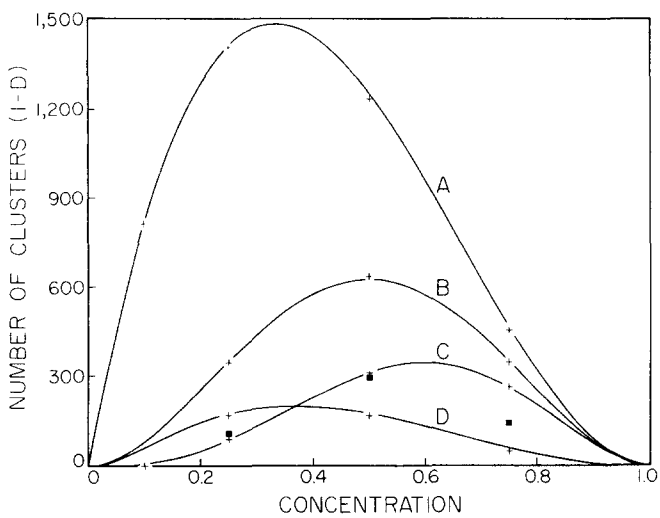

FIG. 18. Theoretical (smooth curves) and computer Monte Carlo values (crosses) for the number of various types of clusters in a 10 000 site linear chain. (A) monomer, (b) dimer, (C) trimer, (D) double monomer. The squares are computer results for the number of directly adjacent monomer and dimer clusters (i.e. GHGGH or GGHGH, not like GHHHGGH). To our knowledge, there is no analytic solution for the number of neighboring monomer and dimer clusters and the results would be difficult to obtain by use of Lagrange multipliers. For all other clusters we have only shown experimental results for 25%, 50%, and 75%. We have exhaustively compared theory and experiment from 1% to 20% and find agreement to *better* than 1%. Error bars are the size of the crosses or smaller.

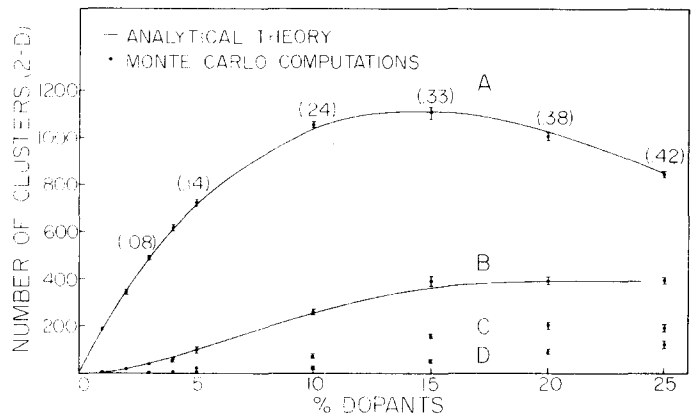

FIG. 19. Two-dimensional Monte Carlo computer simulation for cluster numbers on a 19,500 site lattice. (A) monomer, (B) all dimers (includes TI and TE dimers), (C) total number of trimers (many of which are spatially distinguishable), (D) tetramers. Error bars are the standard deviation of the mean resulting from setting the b-axis parallel to different edges of the computer simulation. Numbers in parentheses are the statistical dimer/monomer ratios from theory. The solid line for curve A is a plot of $C(1-C)^6$; the line for curve B is a plot of $3C^2(1-C)^8$. Although no theoretical expression is available for the larger clusters, workers in the field often use a low density expansion for the perimeter polynomials.[62]

To obtain information about cluster distributions[24-28] in 2-D, we have performed 2-D Monte Carlo calculations on a rectangular 65×300 lattice. Opposite sides of the 65×300 sheet were connected to form a torus in order to: (a) preserve periodic boundary conditions, and (b) eliminate edge effects in counting finite-sized samples. Clusters were counted and dissimilar cluster separations were computed. The prime goal of the 2-D simulation was to mimic the anisotropic phenazine lattice and produce the distribution of impurity clusters as a function of impurity concentration. The results are depicted in Fig. 19.

Over the concentration range from 1% to 25%, the number of monomers precisely fits the functional form of $NC(1-C)^6$, where N is the total number of sites. For the dimer the Monte Carlo results fit $(3.1\pm0.1)NC^2(1-C)^8$. Theoretically,[27] one expects the monomer coefficient [in front of the $NC(1-C)^6$] to be 1 since there is only *one* distinct way to build a monomer on a given site. Similarly, for a dimer the expected coefficient is 3 by symmetry for (2-D) phenazine type systems. This is in good agreement with the Monte Carlo results. Further, for all concentrations investigated, we counted twice as many translationally inequivalent dimers as translationally equivalent dimers. This is reasonable and can be understood by recalling that there are four available TI sites and

two TE sites around each lattice point on which one may build a dimer. Note that the Monte Carlo calculations (a) give the TI/TE ratio, (b) assure us that there is no correlation up to the 5% concentration range that we are dealing with, and (c) provide the cluster separations.

Our Monte Carlo experimental results differ from those of another recent work[28] done on naphthalene, in that we found substantially fewer dimers (our dimer to monomer ratio was smaller by a factor of 1.5 to 2). Note that for a given concentration, their total number of cluster molecules does not add up to the number of occupied sites (even when considering the larger cluster counts which are not displayed). In this work, for each 2-D simulation, the number of clusters was counted and then from the number of clusters of each type, the total impurity count was determined and checked with the expected number of impurities (to be sure that all impurities were accounted for). For a 5% concentration 10 075 site simulation, we have measured the average impurity–impurity separation to be slightly greater than 2.1 lattice constants (using an average lattice constant) with a standard deviation of 1 lattice constant. In other words, the number of intervening host molecules is 1.1. The standard deviation is due in part to the dimers and trimers present which have impurity separations of 1 lattice constant and should not be construed to strictly represent the average fluctuation in distance between *clusters*. We also find for the 5% simulation that the average monomer-nearest dimer separation is slightly greater than 2.6 lattice constants with a standard deviation of 1.

B. The origin of the energy transfer threshold: Percolation vs Anderson transition (AT)

The explanation of the energy transfer "threshold" in disordered molecular crystals is shared by two groups of thought. On one hand Kopelman *et al.*[3] believe in the use of percolation theory to explain the phenomenon. They introduced different kinds of percolation methods (called static, dynamic and sometimes quasistatic percolations). Colson *et al.*,[4] in clear papers, have discussed the validity of such concept to the solids studied in their laboratory and applied the approach to the benzene data.

Klafter and Jortner,[6] on the other hand, have applied Anderson theory of localization[7,8,29–32] and concluded using the Mott argument[8] that percolation[33,34] theory will not be applicable to the case of molecular crystals. We, in our first note,[5] applied Klafter–Jortner (KJ) theory and found good agreement for the phenazine system.

In the Anderson transition approach the threshold concentration is given by [Eq. (5) of Ref. 6]:

$$\bar{C} = 0.25/[\ln(2z\alpha\beta/w)/\ln(\Delta/\beta)+1]^2 , \qquad \text{(IV.3)}$$

where $\alpha \simeq 2.7$ and z (coordination number) $\simeq 4$. w is the inhomogeneous linewidth of the impurity "band," Δ the trap depth and β the nearest neighbor resonance interaction. For phenazine and DBN all these parameters are known.

An important point about the AT is that it is a theory for the zero-Kelvin limit. As the above equation depicts, there is no temperature dependence for $\bar{C}$. Also, the impurity–impurity coupling may be nonuniform. This fact was realized by KJ and they introduced off-diagonal disorder to account in part for this problem. We, in our note,[5] bypassed the phonon problem by introducing a *kinetic model* for trapping and detrapping among the monomers and dimers at high temperatures. (A connection between this model and the model discussed here will be made in the coming section.) But, we did not know how to connect the very low temperature (AT) limit with the high temperature kinetic model.

It seems that by use of the percolation approach or the AT approach one is able to predict a threshold for the transfer of energy. The question we are therefore faced with is: which of the two approaches is adequate for molecular crystals?

Mott[8] has argued against the use of percolation theory in microscopically homogeneous systems. If the ensemble does not show "local" inhomogeneities or near-macroscopic clustering, then macroscopically the transfer of electrons by quantum mechanical tunneling effects prevail. As a result, Mott and others have argued that the inhomogeneous broadening of the solid relative to the bandwidth will be an important factor in determining the formation of extended or localized states (in other words, the Anderson Model).

The other advocates say that even though inhomogeneous broadening may be important, there are two problems in applying AT to organic crystals: the finite lifetime of the trap state and the small bandwidth expected in molecular crystals in triplet states. KJ have shown that the former point can explain the change in the threshold for the transfer, depending on whether $k_t\tau \gg 1$ or $\ll 1$, where k_t is the trapping rate constant and τ is the lifetime. In other words, there is no conflict between the finite lifetime and the concept of using AT. As for the second point, KJ have calculated a bandwidth on the order of 10^{-2} cm^{-1}. Kopelman *et al.*[35] argued that this number should be 2×10^{-8} cm^{-1}. As we shall see later, our calculation agrees with those of KJ. A check on these calculations is made by comparing the analytical result with computer calculations done for diagonal disorder and off-diagonal disorder.[36,6] The results agree to within an order of magnitude with the configurationally averaged results of KJ and of ours, but differ by five orders of magnitude from the 2×10^{-8} cm^{-1} naphthalene result. Finally, it is clear that these organic mixed crystals are inhomogeneously broadened. We are not arguing that the presence of inhomogeneous broadening alone means that we should use AT and not percolation, but we are saying that its presence *together* with the reasonably large impurity bandwidth support, but does not prove, the application of AT to the phenazine system, as we shall discuss later.

V. DISCUSSION OF THE PHENAZINE AND DBN RESULTS

A. Impurity bandwidth from knowledge of β, Δ, and $\langle r \rangle$

To calculate β from the observed M–D splitting we[11] diagonalized a large cluster matrix[37–39] to correct for

the quasi-resonance interactions between guest and host molecules.

In order to calculate the average spatial separation between impurities and thus the average impurity–impurity interaction energy ("bandwidth"), we shall use the first moment of a probability distribution function developed by Hertz.[40,41] The application of this distribution to our situation is not exact, since it smooths the anisotropic topology and produces an isotropic impurity superlattice. Clearly, it is possible to calculate the effects of higher moments of the distribution on the impurity bandwidth, but we find the average adequate in view of other approximations made.

We model the near impurity–impurity neighbor distribution as being isotropic, continuous, and unimodal, assuming substitutional impurities to be spatially uncorrelated. By extension of Hertz's results, the distribution function in one dimension is

$$P(r) = e^{-\bar{\rho}r}\,\bar{\rho}\,dr\ , \qquad (V.1)$$

where r is the distance and $\bar{\rho}$ is the average impurity number density per unit length which is equal to the fractional number of impurities divided by the lattice constant, d. Thus, the average separation, $\langle r\rangle$, becomes

$$\langle r\rangle = \int_0^\infty r\bar{\rho}\,e^{-\bar{\rho}r}\,dr = \Gamma(2)/\bar{\rho} = (\bar{\rho})^{-1}\ , \qquad (V.2)$$

where $\Gamma(2)$ is the gamma function of 2. Clearly, the mean number of host sites between impurities $\langle n\rangle$, is equal to $[(\langle r\rangle/d) - 1]$. Similarly, for 2-D we have $\langle r\rangle = \frac{1}{2}(\bar{\rho})^{-1/2}$, where $\bar{\rho}$ is now the impurity number density per unit area. One should notice that the average distance is inversely proportional to root of the impurity density; at higher densities, $\langle r\rangle$ is shorter. Furthermore, the distribution for the 2-D case is not symmetrical about its mean. The standard deviation about the mean can be calculated in terms of the first and second moments: $\sigma = 0.26/\sqrt{\bar{\rho}}$.

We now make bandwidth calculations specific to the phenazine system. In order to use the statistical formulas we need an average lattice constant for phenazine, and shall use the geometrical average, d, of **a** and **b** (such that the cell area is conserved) which is $(|\mathbf{a}||\mathbf{b}|)^{1/2} = 8.2$ Å. We compute $\langle r\rangle$ for $C = 0.05$, $d = 8.2$: $\langle r\rangle = \frac{1}{2}(\bar{\rho})^{-1/2} = \frac{1}{2}(C/d^2)^{-1/2} = 18.3$ Å. Immediately, $\langle n\rangle = 1.23$, which is likely an underestimate of $\langle n\rangle$ due to neglect of clustering effects in the continuum distribution. $\sigma = 1.1$ lattice constants. This is in good agreement with our Monte Carlo result of $\langle n\rangle$ slightly greater than 1.1. The distribution of cluster separations for the 2-D Monte Carlo is depicted in Fig. 20.

Now that we can calculate average distances, the interaction energy between impurities, and hence the bandwidth (B) can be calculated. At zero Kelvin there is no thermal promotion into the host band and the transfer may proceed through tunneling in the host barriers which are located at $+\Delta$ from the impurity monomer. This tunneling mechanism formulated first by Nieman and Robinson[42] has recently been used for treating exciton percolation,[3,4] exciton coherence,[43] and trap-to-trap

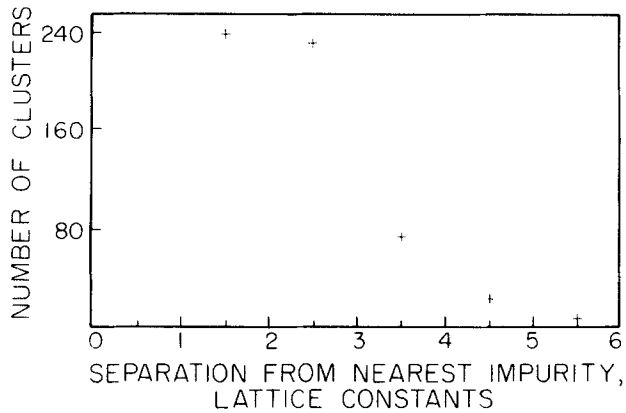

FIG. 20. A bin-sort plot of nearest particle separations in the anisotropic 2-D phenazine lattice. All particles whose nearest neighbor is between one and two lattice constants away are summed to give the first point, all particles whose nearest neighbor is between two and three lattice constants away are summed to give the second point, and so on. Despite clustering effects, the distribution is not too different than that of Fig. 19.

energy transfer.[4,42,44] The idea behind this coupling scheme is simple, but accurate calculation is more difficult for anisotropic 2-D and 3-D systems, and also in cases where the two traps have different energies.

For a linear chain of n intervening host (H) sites separating two monomer traps (M1) and (M2), $J(B/2z)$ takes a simple form[42,4]:

$$J_n = (F_{M1}\beta_0)(F_H\beta_0)^{n-1}(F_{M2}\beta_0)\Delta^{-n}\ ;\ F\beta_0 \ll \Delta\ , \qquad (V.3)$$

where F_M and F_H are, respectively, the Franck–Condon factors for the monomer and the host. β_0 is the nearest neighbor (pure electronic interaction) matrix element and is assumed to be the same for M–H, H–H, and H–M coupling. Colson *et al.*[4] have presented formulas for cases where the two traps are much different in energy. In this case β_0 of the host to the lowest energy trap is generally different from β_0 of H–H, since the lowest energy (or super) trap is chemically different from the host molecules. Because of the large energy gap between the trap and the supertrap, additional Franck–Condon factors were added to account for the mismatch in energy. However, later on in their calculation they have assumed that terms in front of $(F\beta_0/\Delta)^n$ simply give a constant of one [see expression (III.8) in their paper].

We treat the energy transfer between the two impurities (in our case the monomer and dimer) which are separated by only 4 cm^{-1} as a "resonant" process among the monomers, accompanied by absorption (or emission) of phonons of the lattice. (As we shall see later, the results are satisfactory and explain many of the experimental features of the temperature-dependent studies.) The average value of J is therefore:

$$\langle J\rangle \simeq \langle \beta^{n+1}\Delta^{-n}\rangle \simeq \beta^{\langle n\rangle+1}\Delta^{-\langle n\rangle} = \beta\, e^{-\alpha\langle n\rangle}\ ;\ \alpha = \ln(\Delta/\beta)\ . \qquad (V.4)$$

This averaging is not exact but its accuracy can be tested as we did elsewhere.[65]

The value of β in the above expression is difficult to ascertain for anisotropic lattices. However, we shall perform two calculations to show the dependence of J on β. In the first calculation we simply use the 6 cm^{-1} value for β. In this case $J = 1.2$ cm^{-1}. The second calculation is for an effective β that is explicitly determined by β_1 and β_2.[45] Thus we have for this case, $J = 0.1$ cm^{-1} since $\beta_{eff} = \sqrt{6 \times 0.5}$. The important point here is that the calculation is only accurate to an order of magnitude, but provides a value for J (note $B = 2zJ$) and hence B that is orders of magnitude larger than the value calculated by Kopelman *et al.*[35] (2×10^{-8} cm^{-1}) for naphthalene and "comparable" with the value of KJ. For DBN see Ref. 65.

B. Population transfer

1. The kinetics model

The use of a kinetic model that describes population transfer at finite temperatures was first suggested by us in Ref. 5. Here, we wish to make the model properly treat the phonon-induced breakdown of the threshold (here, by breakdown, we mean phonon assisted energy transfer to the host and back to other impurities or between impurities). The question we need to answer is, can we justifiably make approximations in the coupled nonlinear rate equations for the lattice (which we can write down but not solve) to produce a set of soluble rate equations which describe the important physics?

The applicability of kinetics is an old question and has been of concern to many investigators.[46–48] The real problem is due to the dispersion of the impurities in nonequivalent ways. Hence, the interaction matrix elements are a function of **r** (intercluster separation). Statistically the system is not stationary (i.e., depends upon the choice of origin) and usually severe configurational averaging is required. If all the impurities have essentially the same separation, then the population scheme is adequate, otherwise, one must calculate probabilities of finding excitation on a subset of impurity sites and then average over all lattice configurations. Even in one-dimensional systems, the distribution function as a function of **r** is complex. Only recently has this problem been dealt with by Orbach and co-workers[47] to provide macroscopic dynamic rates in terms of microscopic quantities. For our steady state experiments we shall assume that the averaging simply gives rates that are products of population and rate constants.

2. System description

To obtain theoretical expressions relating the observed ratio of dimer to monomer phosphorescence emission to the temperature and the concentration we consider a model system consisting of a host band and two sets of impurity states, and consider transitions between all these levels. We consider that the triplet host band is populated by, e.g., intersystem crossing from the singlet manifold, while the impurity states are populated by a nonradiative phonon emission process from the host band. In addition, we also allow

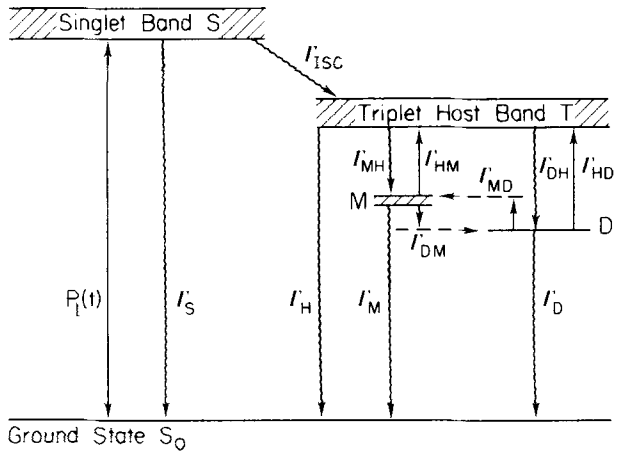

FIG. 21. Level scheme used for kinetic equations (see text for explanation of symbols). This level scheme neglects trapping of singlet excitons, which is appropropriate if the intersystem crossing rate is greater than the singlet exciton trapping rate (see the work of L. J. Noe, E. O. Degenkolb and P. M. Rentzepis.[63])

the possibility of the reverse phonon absorption process which serves to depopulate the monomer and dimer cluster states. These two nonradiative processes establish communication between the host and guest states, and indirectly between the guest states. In crystals with impurity concentrations above a certain transition threshold, the guest states are "extended" and it becomes necessary to consider a direct communication between monomer and dimer clusters. This communication is also treated as a nonradiative transition involving phonon emission (for monomer-to-dimer transitions) and absorption (dimer-to-monomer).

The population of the monomer and dimer levels are found by solving a set of rate equations for the populations of the various levels. The observed emission ratio is simply related to the population ratio through the radiative rate constant. The rate constants for the phonon assisted transitions are calculated in a "Golden Rule"-like form from a knowledge of the intersite coupling and the exciton–phonon coupling Hamiltonian and the phonon occupation numbers which contain the temperature dependence. As described before, the concentration dependence is contained in the spatial probabilities for finding host molecules, monomer or dimer clusters in a random lattice.

The energy level scheme we consider for the various processes under study is shown in Fig. 21. In this figure Γ_S, Γ_H, Γ_M, and Γ_D are the total decay rates to the ground state and contain the radiative and nonradiative contributions. All the other rates are represented by Γ_{ij} which describe a process of excitation transfer *from* j *into* i, where i and j label the host and impurity states. The singlet band is pumped by light, represented by a function $P_L(t)$, the number of transitions into the singlet state, S, per unit time. We assume that the triplet states are not pumped directly by the exciting light, and that the effect of spin splittings, which are much smaller than the inhomogeneous linewidth, is not important. Also, we ignore the effect of singlet traps.

3. Master expressions

Using the notation developed above, we arrive at the average rate equations describing population of the levels in Fig. 21:

$$\dot{n}_M(t) = \Gamma_{MH}\, n_H(t) + \Gamma_{MD}\, n_D(t) - \bar{\Gamma}_M\, n_M(t)$$
$$\dot{n}_D(t) = \Gamma_{DH}\, n_H(t) + \Gamma_{DM}\, n_M(t) - \bar{\Gamma}_D\, n_D(t)$$
$$\dot{n}_H(t) = \Gamma_{ISC}\, n_S(t) + \Gamma_{HM}\, n_M(t) + \Gamma_{HD}\, n_D(t) - \bar{\Gamma}_H\, n_H(t)$$
$$\dot{n}_S(t) = P_L(t) - (\Gamma_S + \Gamma_{1SC}) n_s(t)\ , \qquad \text{(V.5)}$$

where

$$\bar{\Gamma}_i = \Gamma_i + \sum_{i \neq j} \Gamma_{ji} \quad (i,j = \mathrm{M, D, H}) \qquad \text{(V.6)}$$

was used to simplify the notation by indicating the sum of all decay channels for the ith level. All transition rates Γ contain the information on the final density of states, temperature, and energy mismatch. We find the steady state solution to be

$$n_H = (\bar{\Gamma}_M \bar{\Gamma}_D - \Gamma_{MD}\Gamma_{DM})/\theta$$
$$n_M = (\Gamma_{DH}\Gamma_{MD} + \Gamma_{MH}\bar{\Gamma}_D)/\theta$$
$$n_D = (\Gamma_{MH}\Gamma_{DM} + \Gamma_{DH}\bar{\Gamma}_M)/\theta\ , \qquad \text{(V.7)}$$

where

$$\theta = \bar{\Gamma}_S[\bar{\Gamma}_H(\bar{\Gamma}_M\bar{\Gamma}_D - \Gamma_{DM}\Gamma_{MD}) - \Gamma_{HM}(\bar{\Gamma}_D\Gamma_{MH} + \Gamma_{MD}\Gamma_{DH})$$
$$- \Gamma_{HD}(\bar{\Gamma}_M\Gamma_{DH} + \Gamma_{MH}\Gamma_{DM})]/\Gamma_{1SC}P_L\ . \qquad \text{(V.8)}$$

The host singlet pumping and decay terms cancel upon taking the ratio of n_D and n_M, giving

$$n_D/n_M = (\Gamma_{MH}\Gamma_{DM} + \Gamma_{DH}\bar{\Gamma}_M)/(\Gamma_{DH}\Gamma_{MD} + \Gamma_{MH}\bar{\Gamma}_D)\ . \qquad \text{(V.9)}$$

Equation (V.9) is the principal result by which we model the concentration and temperature dependence of the experiment. In the low concentration limit, where Γ_{MD}, $\Gamma_{DM} \to 0$, one finds that equation (V.9) reduces to the following:

$$n_D/n_M = \Gamma_{DH}(\Gamma_M + \Gamma_{HM})/\Gamma_{MH}(\Gamma_D + \Gamma_{HD})\ , \qquad \text{(V.10)}$$

which, at $T \simeq 0$, further simplifies to the ratios of the feeding rate to the decay rate, a familiar result:

$$n_D/n_M = (\Gamma_{DH}/\Gamma_D)/(\Gamma_{MH}/\Gamma_M)\ . \qquad \text{(V.11)}$$

At high concentrations and low temperatures (inefficient detrapping) (V.9) becomes

$$n_D/n_M = [\Gamma_{MH}\Gamma_{DM} + \Gamma_{DH}(\Gamma_M + \Gamma_{DM})]\Gamma_{MH}\Gamma_D\ , \qquad \text{(V.12)}$$

which demonstrates that any increase in trap feeding rates will *increase* n_D/n_M as all population ultimately ends up in the lowest lying state. Also, an increase in the dimer decay rate will reduce the dimer population relative to the monomer.

There are limitations to the kinetic description of the phenazine system—we enumerate a few: (1) The host band states are treated as *one* level, thus the nature of energy transport via host states is not known; (2) Use of discrete levels rather than inhomogeneously broadened levels which hopefully reflect effective energies for phonon assisted energy transfer; (3) Coherence effects are lost in a kinetic scheme, but they may not be important due to disorder; (4) Second and higher order electronic (e.g., multi-impurity energy exchange) and vibrational processes are omitted. Though the importance of the multiphonon processes has been demonstrated in other systems,[49] we presume that the cross section for these processes in band-trap interactions is relatively small; and (5) The dimer (–) state has been omitted which has an undetermined role as an intermediate or final state in energy migration.

4. Role of exciton-phonon coupling: The rate constants

The parameters appearing in Eq. (V.5) are rate constants for two types of processes—transitions between impurity states and host states, and transitions between different impurity states. We adopt the point of view that these transitions are mediated by the electron–phonon interaction.[50]

In the dilute crystal limit (say, one impurity per million host molecules) one may use the standard exciton–phonon formalism[51] of the pure crystal (i.e., crystals with well defined exciton k states) to describe the coupling terms explicitly. This has been recently done by Craig and his collaborators.[52] In the heavy doping limit this simple picture which utilizes the translational symmetry of the *almost* perfect lattice breaks down. Since there is no data that will allow us to compute the coupling terms[53,54] accurately, we shall not elaborate on this point in this article. Rather, we shall express the rates in terms of these coupling parameters like $\partial V/\partial R$, where V is the interaction potential and R the displacement for an electron-phonon interaction.[54]

Using the above results, we can write Γ's at any *temperature* in terms of the concentration of the final species, assuming that the transition started from an averaged state. For example, for Γ_{DM}, the rate involves transitions from equally averaged monomer states to all possible dimers. To conserve the energy a phonon must be emitted during this process. Thus for a single phonon process we may write

$$\Gamma_{DM} = \frac{2\pi}{\hbar}|\Omega_{DM}|^2\rho(\bar{\eta}_q + 1)C_D \qquad \text{(V.13a)}$$

$$\Gamma_{MD} = \frac{2\pi}{\hbar}|\Omega_{MD}|^2\rho(\bar{\eta}_q)C_M \qquad \text{(V.13b)}$$

$$\Gamma_{MH} = \frac{2\pi}{\hbar}|\Omega_{MH}|^2\rho(\bar{\eta}_q + 1)C_M \qquad \text{(V.13c)}$$

$$\Gamma_{HM} = \frac{2\pi}{\hbar}|\Omega_{HM}|^2\rho(\bar{\eta}_q)\ , \qquad \text{(V.13d)}$$

where Ω is the coupling matrix element[55] between, say, the monomer and the host which results in transfer and emission of a phonon with occupation number $\bar{\eta}_q$. Note that Ω_{DM} and Ω_{MD} include J of equation (V.3). The phonon q has the appropriate energy to match H–M, H–D, or M–D energy separations. Finally,

$$\bar{\eta}_q + 1 = (e^{\hbar\omega_q/kT} - 1)^{-1} + 1\ . \qquad \text{(V.14)}$$

Again, we should emphasize that we have assumed constant *microscopic* coupling constants between impurities and made the configurational average discussed before.

C. Numerical simulation of the experiment

In order to test the correctness of the model (described above) in predicting the steady state experiments, we have performed numerical simulations of D/M vs C and $1/T$. An algorithm for the master rate equation (V.9) was written and plots to simulate the experimental data as a function of various parameters were generated. There are six parameters in the kinetic equation, all of which, in principle, can be determined spectroscopically. The parameters are (a) relaxation rates for the monomer, dimer, and host, and (b) coupling constants for transfer between all pairs of the three levels—monomer, dimer, and host.

An attempt was made to fit the experimental curves, D/M vs concentration and temperature, by nonlinear regression for a *fixed* set of relaxation parameters and educated guesses for the coupling constants, but no convergence was obtained, indicating at least for the starting guesses supplied, no unique solution existed (the kinetic expression is too complex to have ascertained this beforehand). Instead, we followed the behavior of the equations for reasonable parameters with self-consistency.

The best simulation of the experimental data using expression (V.9) is shown in Figs. 22 and 23. For phonon-induced transitions, the Hamiltonian for electronic distortion, $\partial V/\partial R$, is implicitly part of Ω. Thus, in addition to J, the phonon occupation number and the concentration, the rate constants have an additional constant, K, that depends on the density of final states, $\hbar$, $\partial V/\partial R$, etc. This "coupling" constant K was a parameter (cm^2/sec) in our fit.

As mentioned before, J depends on $\langle n\rangle$ and for phenazine this is given by

$$\langle n\rangle = (0.5/\sqrt{C}) - 1 \quad .$$

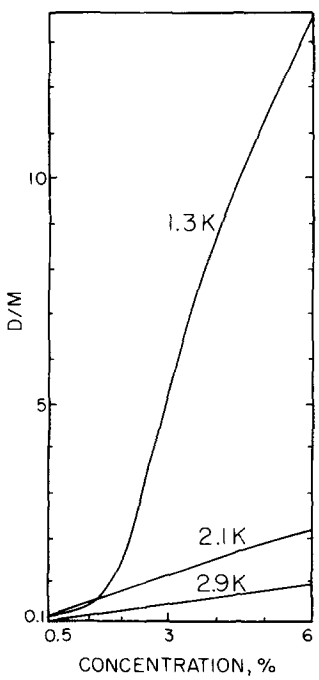

FIG. 22. Theoretical simulation of D/M vs C for phenazine. Rate equation (V.9) was used with the following parameter set: $\Gamma_H = 10^3$, $\Gamma_M = 10^2$, $\Gamma_D = 2\times10^2$, $K_{HM} = 10^{11}$, $K_{HD} = 2\times10^{12}$, $K_{MD} = 3\times10^8$. The monomer trap depth was 18 cm^{-1} (rather than 23 cm^{-1}, using the results of Fig. 14), dimer trap depth was 22.4 cm^{-1} and $\beta/\Delta = (4.4/18)$. The actual rate constants are the product of the fitting parameter, a concentration and a phonon term. Γ_H, Γ_M, and Γ_D are in sec^{-1}.

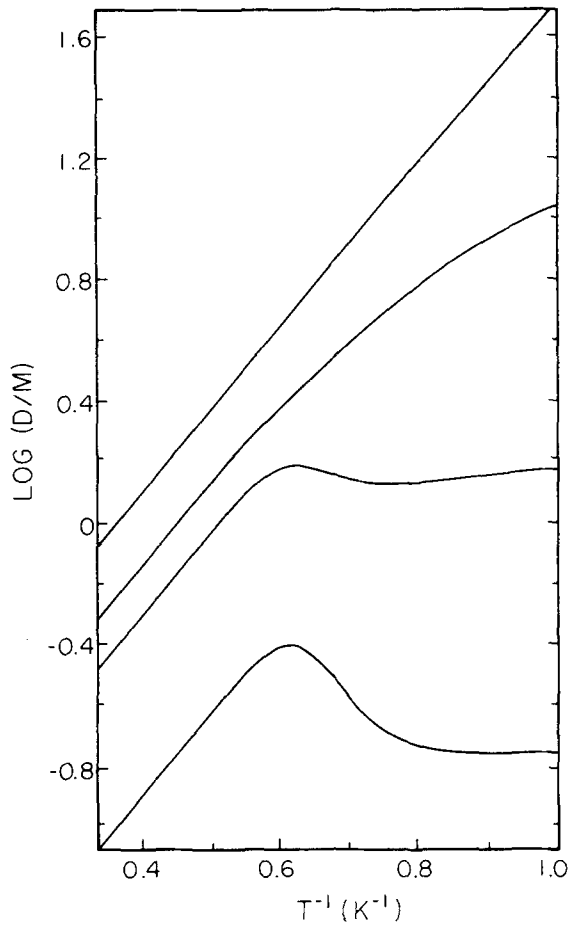

FIG. 23. Theoretical simulation of D/M vs T^{-1} for phenazine using the same parameter set as that of Fig. 22.

In general, Γ_{MD} and Γ_{DM} are related by the ratio of phonon absorption and emission rates (at the energy of mismatch between M and D) and the total concentration of each M and D. Monomer-to-monomer transfer is faster than M-to-D transfer partly due to the relative concentrations. For low C, approximately C of the monomers will be replaced by dimers. Monomer to dimer transfer will predominately occur from monomers directly adjacent to dimers. For monomers not close to a dimer, M-to-M transfer will predominate, but this will not affect the steady state M-to-D transfer, as all monomers in the configuration averaged lattice have the same time-average probability of being excited. The claim that $r_{MD} \simeq r_{MM}$ is substantiated by a Monte Carlo result of $r_{MM} = 2.1$, $\sigma_{MM} = 1$, $r_{MD} = 2.6$, $\sigma_{MD} = 1$ (all in units of lattice constants) for a 5% doped array.[56] Thus, as the monomer bandwidth increases, so does the monomer–dimer coupling. Recall in the concentration range we are interested in, C_D always is less than C_M (C_D/C_M ranges between 5×10^{-2} and 1×10^{-3}).

Figure 23 shows the theoretical log(D/M) vs $1/T$ for the same crystals as Fig. 10 (the two figures should be compared closely). *Curve E(F) for the 0.5% crystal, represents the limit where monomer–dimer communication through the host band prevails.* Indirect communication (illustrated by the results of Fig. 14 on d_8) is frozen out at low temperatures as is evidenced by the

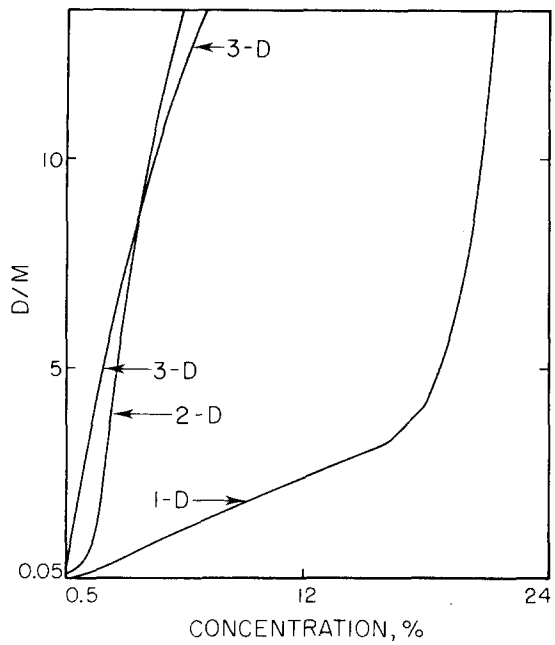

FIG. 24. Calculation of D/M vs C using the rate equation and parameters used to generate Fig. 22, *but* with rate constants modified to represent energy transfer for 1-D and 3-D topologies. Note that the energy transfer threshold moves to decreasing concentration with increasing dimensionality. For the 3-D calculation $\langle n\rangle = 0.554/(C)^3 - 1$, $C_m \propto C(1-C)^6$ and $C_D \propto C^2(1-C)^{10}$ (for a simple cubic lattice structure). Beyond the energy transfer threshold, $D/M \propto (C_D/C_M)e^{\Delta_{MD}/kT}$ and the crossing of the curves 2-D and 3-D results from the terms of the form $(C_D/C_M) \propto C(1-C)^4$ in 3-D and in 2-D $(C_D/C_M) \propto C(1-C)^2$, which are important at higher concentrations.

plateau for $1/T$ greater than 0.6 K^{-1} where the D/M ratio is determined by the statistical probabilities of finding the clusters and their feeding and decay rates [Eq. (V.10)]. Experimentally, the plateau is not completely established at $1/T = 0.8$ K^{-1}, but it seems reasonable that the asymptotic behavior of theory and experiment will coalesce. Also, for the 0.5% crystal, the high temperature "bump" (A of Fig. 23) is predicted (~ 0.5 K^{-1}) but has yet to be experimentally verified due to the weak signal at high temperatures (bear in mind S/N greater than or equal to 100 is necessary to accurately measure the intensity of weak dimer satellite peak).

The importance of the 0.5% data at low temperatures is that they demonstrate the localized nature of the excitation and the departure from Boltzmann statistics. The usual partition function approach is no longer useful at these concentrations and temperatures. Furthermore, at these low concentrations and temperatures the rate equations must include trap-"band" interactions,[57] especially in phenazine-type systems where Δ is relatively small.

The 2% crystal demonstrates a low temperature plateau but no bump as predicted theoretically. The plateau for the 2% case cannot be taken to imply "locality" of states, however. The physical significance of the lack of a bump in the high concentrated crystals lies primarily in the fact that the monomer and dimer communicate directly. These conclusions were arrived at by detailed inspection of the numerical results used to produce Fig. 23. For the 0.5% crystal at higher temperatures, the monomer indirectly feeds the dimer and to a much smaller extent the dimer feeds the monomer indirectly. The dimer to host detrapping transfer freezes out before the monomer detrapping resulting in the "negative activation energy" seen in the 0.5%. The plateau is due to freezing out of both channels of communication. The value of D/M at these low concentrations and at $T < 1$ °K will be determined by Eq. (V.10).

The extreme nonlinearity of the phonon occupation number at ultralow temperatures is the key to understanding the changes. The monomer detrapping rate changes by 10 orders of magnitude from 1 to 4 °K and the dimer changes by 12 orders of magnitude from 1 to 4 °K. In the 2% crystal, the dimer is not truly isolated from the monomer (therefore no bump) and the kinetic equations dictate the largest D/M ratio should occur when there is no appreciable dimer to monomer back transfer (i.e., the low temperature plateau) which is jointly a function of the electronic matrix element, phonon occupation number, and final density of states.

For the 3% and 6.6% crystals, the increase in the tunneling matrix element is primarily responsible for the disappearance of the plateau at these temperatures. However, if one calculates D/M for T less than 1 °K, one finds that even the 6.6% has an asymptotic temperature-independent value.

Theory predicts that at high temperatures, $T > 2$ °K, the D/M ratio should be Boltzmann-like with an activation energy of 4.4 cm^{-1} for *all* crystals. This can be seen [from Eq. (V.9)] to occur as a result of direct (high-concentration) or indirect (low-concentration) communication between M and D. As an example, in the strong direct communication limit, equation (V.9) simply yields

$$n_D/n_M \propto e^{\Delta_{MD}/kT}$$

where Δ_{MD} is the monomer–dimer splitting. Note that the above findings are consistent with the results of Fig. 22 (D/M vs C at different temperatures) which reproduce the experimental observations. Further, the measured activation energy indicates that for first order detrapping processes, the dimer (–) state is not likely to be an important intermediate state.

We have thus advanced explanations for the D/M ratio as a function of concentration and temperature. A numerical simulation of the absolute cluster intensities as a function of concentration and temperature was also conducted in order to test the model. It is difficult, however, for the choice of the many parameters to place much certainty on such computation. Nevertheless, we shall make some heuristic observations on the data.

One can see that for the monomer intensity as a function of temperature (Fig. 13) a trend of decreasing emission with increasing T dominates all samples and

is most pronounced for the d_8 phenazine crystal. For this "pure" d crystal, one has a steep decline in intensity that shows an 18 cm^{-1} activation energy (Fig. 14). The 18 cm^{-1} activation energy is less than the trap depth measured to the lowest available $k=0$ state (21 cm^{-1}).[1] This may be understood by noting that quasiresonance interactions create states *below* the band by several wave numbers.[58] Thus detrapping can occur to lower energy host states. The observed 18 cm^{-1} activation energy also implies that the population lost by detrapping to the host is lost forever to the monomer subsystem. This is intuitive insofar as the average monomer–monomer separation should be so large that transport between monomers via host states is not successful. The 0.5% phenazine crystal is unlike the "pure" d_8 case in showing much less dependence on temperature, implying that to some extent indirect monomer-to-monomer transfer[56] occurs and population is *not* irreversibly lost to the host. Looking at the remainder of the data in Fig. 13, one sees that the monomer system loss rate appears to decrease with increasing guest concentration (up to 2%). However, for a detailed description of the population of the monomer which lies between the band and the dimer, one must know all the *direct* and *indirect* communication parameters given in θ of Eq. (V.8). We feel that a simulation is not useful at this point and only the ratio of M to D can be satisfactorily explained.

For the dimer emission as a function of temperature, the situation is different (the dimer is the deepest trap under consideration). For the 0.5% phenazine crystal, dimer population *increases* with increasing temperature over the range 1.0 to 1.2 °K (rather than decreasing as the monomer does). This behavior is correctly represented by the rate equations and can be understood as indirect M to D transfer with little back transfer. The trend may only be exhibited over a narrow temperature range where the dimer detrapping rate is still small in comparison to the monomer detrapping rate and thus presents an "irreversible" sink for monomer population. The 2% and 6.6% cases would then represent situations where the dimer to monomer back transfer increases as temperature increases. The dimer and trimer in the 6.6% crystal appear to decrease in a linear fashion with increasing T. This is not explicable by a naive model where the ratio of the dimer feeding rate to dimer decay rate is written as $(\bar{\eta}+1)/\bar{\eta}$. Such a model would predict exponential temperature dependence which is beyond our error bars, even for a 4.4 cm^{-1} activation energy. In actuality, this behavior reflects the complexity involved in using absolute intensities which require knowledge of θ. In other words, to describe this linearity quantitatively we must solve the full kinetic equation. As mentioned before, taking the ratio of D/M overcomes this problem.

For DBN, the log(D/M) vs $1/T$ plots show the expected trends derived from the phenazine analyses, although we feel one must have more data over a wider temperature range before making quantitative interpretations (this is currently under investigation). It does appear, however, that the D/M ratio is roughly temperature independent for low concentrations and begins to show positive activation energies for higher concentrations, in accord with direct communication between monomer and dimer.

The "sluggishness" of the D/M threshold in DBN with concentration (Fig. 9) is due largely to the smaller exponent for the superexchange coupling which goes as $(C^{-1}-1)$ for 1-D and $(0.5/\sqrt{C}-1)$ for 2-D. As a means of illustrating this point, we have performed a simulation of D/M ratios for the phenazine system parameters, altering only the form of the macroscopic rate constants of Eq. (V.9) to represent a 1-D and 3-D system.

We compute D/M vs C for the different dimensionalities and compare them in Fig. 24. In altering the rate constants for the 1-D and 3-D cases, one must change the exponent in the superexchange matrix element and the concentration of the final state. We use $\langle n\rangle = C^{-1}-1$ in 1-D and $\langle n\rangle = 0.554\,C^{-3}-1$ in 3-D. The final specie concentration in 1-D follows the prescription in Sec. IV and in 3-D we use a simple cubic lattice [coordination number 6, monomer $\propto C(1-C)^6$ and dimer $\propto C^2(1-C)^{10}$]. The energy transfer threshold moves to decreasing concentration with increasing dimensionality largely due to the increased probability of finding a nearby impurity at short distance. However, the change in concentration of the final state as a function of dimensionality (at least with the form of rate equations we use) works against the effect of change in the superexchange exponent. That is, an increase in lattice dimensionality (or connectivity) increases the superexchange coupling but reduces final state concentrations due to terms of the form $C^n(1-C)^h$ (n is the cluster size and h is the number of host molecules on the cluster perimeter, which increases with dimensionality). The results of Fig. 24 are consistent with the results of ruby, phenazine and DBN.

Two important conclusions can now be drawn. First, the fact that we can fit the results at very low temperatures (no thermal assistance) with an effective tunneling matrix element between M and D indicates that the threshold concentration is most probably the result of this quantum effect. Second, from the parameters used in the simulation, at 5% and 1 K, $\Gamma_{DM}\tau$ is 10^3, much larger than 1 (τ is the lifetime). Hence, the threshold is not lifetime limited. At higher temperature this situation is different simply because of the back transfer discussed before (Γ_{MD} at 2 °K, 5% is about 8×10^5 sec^{-1}).

VI. SUMMARY AND CONCLUSIONS

We have presented data on isotopically doped phenazine (effective 2-D) and DBN (effective 1-D) concentration and temperature dependent optical emission. By use of an average-lattice rate equation and a numerical simulation of the data we have presented explanations for much of the data. To properly execute the simulation we have performed Monte Carlo calculations on cluster statistics in one and two dimensions and have calculated the eigenstates of relevant clusters.

From the studies made on phenazine and DBN the following conclusions were drawn: (1) Impurity state populations are sensitive to *all* communication channel rates and the host states must be included to understand the

energy transfer dynamics between impurities, *especially at low concentrations*; (2) The role of the phonon bath in "masking" the threshold at higher temperatures can now be understood; (3) One can understand many of the important processes at hand with a kinetic scheme; and (4) By explicit computation and comparison with experiment (DBN vs phenazine), the important role of *dimensionality* on threshold behavior is also explainable with the same kinetic model. In phenazine, M–D coupling has exponential turn on with concentration which can be modeled by a continuum particle separation distribution to a first approximation. This continuum averaging scheme, although a severe approximation to the discrete anisotropic lattice, appears to explain the steady-state experiments. In transient experiments this may not be the case.[65]

The Boltzmann and non-Boltzmann regimes were delineated and individual trap intensity dependence on temperature and concentration in the 1-D and 2-D systems was experimentally shown and discussed. There are four distinct and limiting cases. In the *low-concentration* (below the abrupt transition), *low-temperature* case, the dimer and monomer population are proportional to their statistical probabilities of occurrence. In the *high-concentration, low-temperature* limit, the monomer-to-dimer transfer is "opened" by monomer-to-monomer extension followed by trapping into a dimer of which there are fewer present (dimers are outnumbered by a factor of 20–1 000). Thus, in this case the population is nonstatistical in the number of clusters, but is statistical when the concentration is weighted by Boltzmann factors that are indicative of efficient and direct communication among clusters (using phonon absorption and emission). In the *high-concentration, high-temperature* limit, the back transfer from D to M (which are in equilibrium due to direct communication) hinders the overall flow of population into the dimer, hence decreasing the ratio of D/M. In the *low-concentration, high-temperature* limit, indirect transfer again makes the dimer and monomer communicate. Because the monomer–dimer energy splitting is the same as the difference in trap depths of the monomer and dimer, phonon absorption and emission ensures the same "activation" energy for the high-concentration, high-temperature and low-concentration, high-temperature regimes. Thus, as shown in Fig. 22 and as demonstrated experimentally, D/M vs C exhibits a straight line at high temperatures.

From the work reported here on DBN and phenazine we determined the temperatures at which phonon-assisted processes are negligible, and thus only the intrinsic effects of energy localization or delocalization are observed. Throughout the paper, only single phonon processes are considered at the temperatures of interest,[59] and radiative transfer is not included.[66]

Finally, we believe that at *very* low temperatures the monomer "band" is extended and wide (~ 0.1–0.01 cm^{-1}) near the transition. As noted in I, our measurement of w, the inhomogeneous site energy fluctuation (Gaussian distribution) and using Eq. (IV.3) predicts a transition from "localized" to "delocalized" states at ~5% concentration, when using the Klafter–Jortner model of the Anderson transition in the phenazine system. This result is consistent with the findings in Fig. 22, which does not include w explicitly. In other words, we explain essentially all the dynamics using the averaged rate equations approach and invoking the superexchange interaction which includes the proper concentration exponent. *This is one of the important conclusions of this paper.* So, the only connection we can make with AT is at very low temperature since our results at 1.17°K is consistent with the KJ model. Experiments are now in progress to elucidate the role of w, especially at higher temperatures.

Note added in proof: Very recently A. Blumen and R. Silbey (private communication of a preprint) have considered a simple kinetic scheme. Three things are different: (1) They consider the case of direct population of the monomer and no direct population of the dimer. In our 1977 note (see Ref. 5) and this work we considered the situation where the rates at which the monomer and dimer are populated are both finite. This is because the experiments on phenazine were performed at steady state by pumping the host states and not the monomer alone. (2) They describe the electronic energy transfer using the hopping model of Inokuti and Hirayama (J. Chem. Phys. **43**, 1978 (1965)). (3) No host states are included in their model. Due to the omission of the host states it is unlikely that the model of Blumen and Silbey could treat the 0.5% phenazine data properly. At higher concentrations, however, their model fits the data well. As shown in this paper the host states of phenazine play a very important role in the energy transfer process, especially at low concentrations (2%, 0.5%, pure d_8). We believe that the communication channels described in Fig. 21 must be invoked since the trap depth is only 23 cm^{-1} and it is almost impossible to populate the monomer selectively. In contrast to the work reported here, neither our work in Ref. 5 nor the work of Blumen and Silbey have dealt with the effects of detrapping to host states.

ACKNOWLEDGMENTS

We wish to thank the National Science Foundation (Grant No. DMR77-19578) for the partial support of this work. Acknowledgment is also made to the donors of the Petroleum Research Fund, administered by ACS, and to DOE and Research Corp. for partial support of this work. We have benefitted from discussions with several people: Darryl Smith, J. Lemaistre and Ray Orbach. We wish to thank A. Nichols for the help with the 1-D cluster statistics and computer work. Thanks also go to R. Kopelman and J. Jortner and J. Klafter for providing us with preprints of their work.

[1]For reviews see: G. W. Robinson, Ann. Rev. Phys. Chem. **21**, 429 (1970); R. M. Hochstrasser, Int. Rev. of Science, Phys. Chem. Ser. 2, Vol. 3, edited by D. A. Ramsay (Butterworths, London, 1976).

[2]H. C. Wolf in Adv. At. Mol. Phys. **3**, 119 (1967); R. Silbey, Ann. Rev. Phys. Chem. **27**, 203 (1976); D. Zwemer and C. B. Harris (to be published).

[3]R. Kopelman, E. M. Monberg, F. Ochs, and P. Prasad, J. Chem. Phys. **62**, 292 (1975); R. Kopelman, E. M. Monberg, and F. W. Ochs, Chem. Phys. **19**, 413 (1977); **21**, 373 (1977); R. Kopelman, E. M. Monberg, F. Ochs, and P. Prasad, Phys. Rev. Lett. **34**, 1506 (1975).
[4]S. D. Colson, S. M. George, T. Keyes, and V. Vaida, J. Chem. Phys. **67**, 4941 (1977); *ibid.* **66**, 2187 (1977).
[5]D. D. Smith, R. D. Mead, and A. H. Zewail, Chem. Phys. Lett. **50**, 358 (1977).
[6]J. Klafter and J. Jortner, Chem. Phys. Lett. **49**, 410 (1977); J. Klafter and J. Jortner (to be published).
[7]P. W. Anderson, Phys. Rev. **109**, 1492 (1958).
[8]N. F. Mott, Phil. Mag. **29**, 613 (1974); Comm. Phys. **1**, 203 (1976).
[9]G. L. Pollack, Rev. Mod. Phys. **41**, 48 (1969).
[10]F. H. Herbstein and G. M. J. Schmidt, Acta Cryst. **8**, 399 (1955); **8**, 406 (1955).
[11]A. H. Zewail, Chem. Phys. Lett. **33**, 46 (1975); J. P. Lemaistre and A. H. Zewail, J. Chem. Phys. 72, 1055 (1980).
[12]R. H. Clarke and R. M. Hochstrasser, J. Chem. Phys. **47**, 1915 (1967).
[13]J. Trotter, Can. J. Chem. **39**, 1574 (1961).
[14]R. M. Hochstrasser and J. D. Whiteman, J. Chem. Phys. **56**, 5945 (1972).
[15]R. M. Hochstrasser and A. H. Zewail, Chem. Phys. **4**, 142 (1974).
[16]We have recently observed these and additional new lines as Raman scattering in time resolved laser experiments; unpublished results from this laboratory.
[17]T. G. Pavlopoulos, J. Chem. Phys. **51**, 2936 (1969).
[18]S. Califano, J. Chem. Phys. **36**, 903 (1962).
[19]A. H. Zewail, Chem. Phys. Lett. **29**, 630 (1974).
[20]In DBN the D/M ratio in the 0, 0 relative to 0, v is different from the phenazine case. This may be due to the extent to which vibrational energy delocalization in the two cases occurs.
[21]L. A. Rebane and P. M. Saari, Sov. Phys. Sol. St. **12**, 1547 (1971); S. Colson, Chem. Phys. Lett. 44, 431 (1976).
[22]J. Ph. Grivet and J. M. Lhoste, Chem. Phys. Lett. **3**, 445 (1969).
[23]K. P. Dinse and C. J. Wincom, J. Chem. Phys. **68**, 1337 (1978).
[24]R. B. McQuistan, J. Math. Phys. **12**, 2113 (1971).
[25]D. Stauffer, J. Stat. Phys. **18**, 125 (1978).
[26]P. L. Leath, Phys. Rev. B **14**, 5046 (1976).
[27]M. E. Fisher and J. W. Essam, J. Math. Phys. **2**, 609 (1961).
[28]J. P. Lemaistre, Ph. Pee, R. Lalanne, F. Dupuy, Ph. Kottis, and H. Port, Chem. Phys. **28**, 407 (1978). A private communication with J. Lemaistre revealed that their figure was in error and one should see Ph. Pee, R. Brown, F. Dupuy, Ph. Kottis, J. P. Lemaistre, Chem. Phys. **35**, 429 (1978).
[29]E. N. Economou and M. H. Cohen, Phys. Rev. B **4**, 396 (1971); **5**, 293 (1972); Mat. Res. Bull. **5**, 577 (1970).
[30]G. Theodorou and M. H. Cohen (preprint); E. N. Economou and M. H. Cohen, Phys. Rev. B **4**, 396 (1971); Phys. Rev. Lett. **25**, 1445 (1970).
[31]J. Koo, L. K. Walker, and S. Geschwind, Phys. Rev. Lett. **35**, 1669 (1975), C. Hsu and R. C. Powell, *ibid.* **35**, 734 (1975).
[32]E. N. Economou and M. H. Cohen, Phys. Rev. B **5**, 2931 (1972); Phys. Rev. Lett. **25**, 1445 (1970).
[33]S. R. Broadbent and J. M. Hammersley, Proc. Camb. Phil. Soc. **53**, 629 (1957).
[34]S. Kirkpatrick, Rev. Mod. Phys. **45**, 574 (1973); V. K. S. Shante and S. Kirkpatrick, Adv. Phys. **20**, 325 (1971).
[35]E. Monberg and R. Kopelman, Chem. Phys. Lett. (to be published).
[36]J. Heinrichs, Phys. Rev. B **16**, 4365 (1977); D. Wearie and A. R. Williams, J. Phys. C **10**, 1239 (1977).
[37]H. Hong and R. Kopelman, J. Chem. Phys. **55**, 724 (1971).
[38]A. Ralston and H. Wilf, *Mathematical Methods for Digital Computers*, Vol. II (Wiley, New York, 1967).
[39]For phenazine the Davydov splitting of h_8 and d_8 is the same implying the same β. For DBN we can fit all the aggregate spectra using nearest neighbor approximation, justifying the short range nature of the interaction.
[40]P. Hertz, Math. Ann. **67**, 387 (1909).
[41]S. Chandrasekhar, Rev. Mod. Phys. **15**, 1 (1943).
[42]G. C. Nieman and G. W. Robinson, J. Chem. Phys. **37**, 2150 (1962).
[43]D. A. Zwemer and C. B. Harris, J. Chem. Phys. **68**, 2184 (1978).
[44]M. T. Lewellyn, A. H. Zewail, and C. B. Harris, J. Chem. Phys. **63**, 3687 (1975).
[45]M. H. Cohen, private communication.
[46]W. Grant, Phys. Rev. B **4**, 648 (1971); D. L. Huber, D. S. Hamilton, and B. Barnett, Phys. Rev. B **16**, 4642 (1971); D. S. Hamilton, P. M. Selzer, and W. M. Yen, Phys. Rev. B **16**, 1858 (1977); F. Fong and D. J. Diestler, J. Chem. Phys. **56**, 2875 (1972); V. P. Sakun, Sov. Phys. Solid State **14**, 1906 (1973); S. Haan and R. Zwanzig, J. Chem. Phys. **68**, 1879 (1978); G. W. Robinson (unpublished results); J. A. Altmann, G. Beddard, and G. Porter, Chem. Phys. Lett. **58**, 54 (1978); M. J. Schaffman and M. Silver (preprint); J. P. Lemaistre, Ph. Pee, R. Lalanne, F. Dupuy, Ph. Kottis, and H. Port, Chem. Phys. **28**, 407 (1978).
[47]J. Bernasconi, S. Alexander, and R. Orbach, Phys. Rev. B **17**, 4311 (1978); see also D. D. Dlott, M. D. Fayer, and R. D. Wieting, J. Chem. Phys. **67**, 3808 (1977).
[48]A. Szabo, Phys. Rev. Lett. **25**, 924 (1970); **27**, 323 (1971). L. A. Riseberg, Phys. Rev. A 7, 671 (1973); D. L. Huber, D. S. Hamilton, and B. Barnett, Phys. Rev. B **16**, 4642 (1977); D. S. Hamilton, P. M. Selzer, and W. M. Yen, Phys. Rev. B **16**, 1858 (1977).
[49]T. Holstein, S. K. Lyo, and R. Orbach, Phys. Rev. Lett. **36**, 891 (1976); T. Holstein, S. K. Lyo, and R. Orbach, Comments on Solid State Phys. (to be published).
[50]Electron-phonon coupling is usually used to refer to the interaction between localized excitation on molecules and phonons (even though there is no free electron).
[51]A. S. Davydov, *Theory of Molecular Excitons* (Plenum, New York, 1971).
[52]D. P. Craig and L. A. Dissado, Chem. Phys. Lett. **44**, 419 (1976); Chem. Phys. **14**, 89 (1976).
[53]D. Smith, D. Millar, and A. Zewail, unpublished results.
[54]R. M. Hochstrasser and P. N. Prasad, J. Chem. Phys. **56**, 2814 (1972).
[55]The $\partial V/\partial R$ term represents a "distortion" in the lattice which results in the absorption or emission of phonons, hence a transition amongst crystal states (trapping and detrapping). For H $\rightharpoonup$ M and H $\rightharpoonup$ D the coupling term Ω is given in terms of $\partial V/\partial R$ (and possibly the higher order derivatives) in addition to the single jump resonance interaction matrix element between H and M or D. For D $\rightharpoonup$ M, Ω contains the effective electronic coupling matrix elements, which depend on *concentration*, and the distortion terms, i.e., $\partial V/\partial R$, that will lead into phonon absorption and emission between the monomer and the dimer.
[56]There is a simple physical picture for the average impurity sublattice and it is as follows. Construct a 2-D net with lattice constant $\langle r_{MM}\rangle = 0.5C^{-1/2}$, placing monomers at every corner. Then replace approximately C of the monomers by dimers. Alternatively, superimpose a dimer impurity net with lattice constant $0.5C^{-1}$ which gives a ratio of areas covered by the dimer relative to the monomer of C^{-1} (which is what one expects since the ratio of TE dimers to monomers is $C^2(1-C)^8/C[(1-C)]^6 \simeq C$ for low C). One can see two things; (a) for low C, most monomers will not be near a dimer, and (b) as one increases the concentration, the monomer net shrinks but the dimer net shrinks faster. Thus, for a monomer *not* near a dimer, fewer $m-m$ steps are required to reach a dimer with increasing concentration (the shrinking net ef-

fect is contained in the rate equations' density of states). Further, one should note that the monomer–monomer transfer is probably more efficient than monomer–dimer transfer[65] much as in the case of ruby (G. F. Imbusch, Phys. Rev. **153**, 326 (1967)). Note that $\langle r_{MM} \rangle \simeq 5$ lattice constants for 1% in contrast to 2.2 lattice constants for the 5% crystal.

[57]M. D. Fayer and C. B. Harris, Phys. Rev. B **9**, 748 (1974).

[58]In addition to the host–guest mixing which produces levels below the host band, partially deuterated species (unavoidably present in relatively low concentrations) will have lower energy than that of the perduetero host. For example, in phenazine there is a detectable ~17% d_7 and ~3% d_6 (Table I). If the isotopic energy shift is roughly ($\frac{21}{8} = 2.6$ cm^{-1}) perdeuterium, then the d_6 will be 5.2 cm^{-1} below the lowest $k = 0$ level. Thus, a trap depths for d_6 and d_7 from the h_8 monomer are simply 16 and 18.5 cm^{-1}, respectively. Note that the sample does not contain a detectable d_5, d_4, d_3, d_2, or d_1.

[59]Multiphonon processes, although of lower probability than single phonon processes, may dominate especially when the density of phonon states is low at the one-phonon energy and the "coherence" length, λ_C, of the phonon is much larger than the spatial separation of the impurities, with energy mismatch Δ. The former density of states (and population) depends on Δ and the temperature. The latter, λ_c, depends on the velocity of sound (v) in the crystal; $\lambda_c = \hbar v \Delta^{-1}$. Thus, if λ_c exceeds the separation between, say, the monomer and dimer, then the two impurities will be phonon-modulated to the same extent and the single phonon process becomes inefficient. For DBN, e.g., taking $v = 1 \times 10^5$ cm/sec[60] and $\Delta = 5.5$ cm^{-1}, we obtain $\lambda_c = 60$ Å. At 5% concentration, the separation of c-axis impurities is roughly 80 Å. Thus, single phonons may efficiently assist the transfer. As Δ gets smaller or the concentration gets higher, one expects that this criterion becomes less applicable.

[60]A. Burns and C. B. Harris (unpublished results; private communication). These authors have found from the heat capacity measurement on 1,2,4,5-tetrachlorobenzene crystals at 1.4–2.2 °K that the Debye temperature is 81 °K (52 cm^{-1}) and hence $v = 1.58 \times 10^5$ cm/sec.

[61]*Introductory Engineering Statistics*, Guttman, Wilks, and Hunter (Wiley, New York, 1971).

[62]M. F. Sykes and M. Glen, J. Phys. A **9**, 87 (1976) and references therein.

[63]L. J. Noe, E. O. Degenkolb, and P. M. Rentzepis, J. Chem. Phys. **68**, 4435 (1978).

[64]U. Doberer, Diplomarbeit, University of Stuttgart, Stuttgart, Germany (1978).

[65]D. Smith, R. Powell, and A. H. Zewail, Chem. Phys. Lett. (in press).

[66]Phenazine, in contrast to DBN, has a smaller oscillator strength, such that no radiative self-absorption effects were seen when comparing emission of the (0, 0) and vibronic transitions.